



Effects of structure and volcanic stratigraphy on groundwater and surface water flow: Hat Creek basin, California, USA

Marina F. Marcelli¹ · Erick R. Burns² · L. J. Patrick Muffler³ · Andrew Meigs⁴ · Jennifer A. Curtis⁵ · Christian E. Torgersen⁶

Received: 15 July 2021 / Accepted: 11 September 2022 / Published online: 16 December 2022
This is a U.S. Government work and not under copyright protection in the US; foreign copyright protection may apply 2022

Abstract

Hydrogeologic systems in the southern Cascade Range in California (USA) develop in volcanic rocks where morphology, stratigraphy, extensional structures, and attendant basin geometry play a central role in groundwater flow paths, groundwater/surface-water interactions, and spring discharge locations. High-volume springs (greater than 3 m³/s) flow from basin-filling (<800 ka) volcanic rocks in the Hat Creek and Fall River tributaries and contribute approximately half of the average annual flow of the Pit River, the largest tributary to Shasta Lake. A hydrogeologic conceptual framework is constructed for the Hat Creek basin combining new geologic mapping, water-well lithologic logs, a database of active faults, LiDAR mapping of faults and volcanic landforms, streamflow measurements and airborne thermal infrared remote sensing of stream temperature. These data are used to integrate the geologic structure and the volcanic and volcanoclastic stratigraphy to create a three-dimensional interpretation of the hydrogeology in the basin. Two large streamflow gains from focused groundwater discharge near Big Spring and north of Sugarloaf Peak result from geologic barriers that restrict lateral groundwater flow and force water into Hat Creek. The inferred groundwater-flow barriers divide the aquifer system into at least three leaky compartments. The two downstream compartments lose streamflow in the upstream reaches (immediately downstream of the groundwater-flow barriers) and gain in downstream reaches with the greatest inflows immediately upstream of the barriers.

Keywords Groundwater/surface-water interaction · Volcanic aquifers · Groundwater-flow barriers · Faults as groundwater-flow barriers · USA

✉ Marina F. Marcelli
mmarcelli@usgs.gov

¹ US Geological Survey, California Water Science Center, 4165 Spruance Road, San Diego, CA 92101, USA

² US Geological Survey, Geology, Minerals, Energy, and Geophysics Science Center, 2130 SW 5th Ave, Portland, OR 97201, USA

³ US Geological Survey, Volcano Science Center, 345 Middlefield Road, Menlo Park, CA 94025, USA

⁴ 104 CEOAS Administration Hall College of Earth, Ocean, and Atmospheric Sciences, Oregon State University, Corvallis, OR 97331, USA

⁵ US Geological Survey, California Water Science Center, 716 UNIT E W Cedar Street, Eureka, CA 95501, USA

⁶ US Geological Survey, Forest and Rangeland Ecosystem Science Center, Cascadia Field Station, University of Washington, School of Environmental and Forest Sciences, Seattle, WA 98195, USA

Introduction

The Cascade Range is a primary control of water resources in the Pacific Northwest, USA, dividing the wet western parts of Oregon, Washington, and northern California from the semi-arid eastern parts. Precipitation in the Cascade Range is one of the main sources of water for hydrologic systems on both sides of the mountain range (PRISM Climate Group 2015; Thornton et al. 2016). Groundwater basins within the permeable High Cascades, a relatively young volcanic province with respect to the Western Cascades, are important components of the hydrologic system from both ecological and water-resources perspectives (Gannett et al. 2001; Jefferson et al. 2006, 2010). Groundwater flow paths can take years to decades to connect recharge areas to discharge areas.

The volcanic landscape of the northwestern USA hosts more than half of the high-volume springs (>3 m³/s) of the

conterminous USA (Meinzer 1927). Much of the discharge of these springs originates from the volcanoes of the Cascade Range between Lassen Peak, California, and Mount Rainier, Washington (Meinzer 1927), where annual precipitation can exceed 250 cm/year (Thornton et al. 2016). Springs between Medicine Lake volcano and Lassen Peak (Fig. 1) contribute approximately half of the average annual flow (total flow of ~140 m³/s) to the Pit River, the largest tributary to Shasta Lake, California's largest surface-water reservoir (Meinzer 1927; Burns et al. 2017b). Whereas the Pit River originates to the east of the Shasta-Lassen Peak-Medicine Lake volcano study area (SLMSA, Fig. 1), most of the flow delivered to Shasta Lake accumulates from streams within the SLMSA (Meinzer 1927). As Fall River headwater springs have been the focus of previous hydrogeologic studies (Manga and Kirchner 2004; Davisson and Rose 2014; Burns et al. 2017b), the emphasis of this study is on the hydrogeology of the understudied Hat Creek basin. Two low-volume springs on Lassen Peak's northern flank serve as the Hat Creek headwaters, below which Hat Creek flows about 78 km northward. Additionally, three high-volume spring complexes (Big Spring, Rising River, and Crystal Lake) contribute to Hat Creek before it joins the Pit River (Figs. 1, 2 and 3).

In the SLMSA, groundwater flow paths connect volcanic uplands to streams and rivers through laterally extensive volcanic rocks (Rose et al. 1996), including the numerous springs feeding Hat Creek from young volcanic rocks (Rose et al. 1996; Davisson and Rose 1997; Fig. 2). In the northwestern USA, high-volume springs flow through and from laterally extensive volcanic units (Gannett et al. 2001). High-volume springs in these regions can serve as a stable year-round and drought-resistant water source, as perturbations from changing climate in the groundwater system lag surface-water changes due to long groundwater residence times (Gannett et al. 2001; Burns et al. 2017b). In northern California, average annual flow from these springs typically fluctuates less than 15% (Meinzer 1927).

Purpose and scope

The Northwest Volcanic Aquifer Study Area (NVASA, Curtis et al. 2020) project is a US Geological Survey (USGS) effort to understand and quantify regional water resources in the Pacific Northwest. This manuscript analyzes geologic controls on groundwater flow in the SLMSA (Figs. 1 and 2), the southwesternmost part of the NVASA. To date, an in-depth analysis of the relationship between structure, stratigraphy, and groundwater flow between Medicine Lake volcano and Lassen Peak has not been conducted. The study narrows in on the Hat Creek focus area (Fig. 1), one of the

principal contributors to Shasta Lake, the largest reservoir in California (Figs. 1 and 2). The relationship between structural geology, volcanology, groundwater recharge, and stream hydrology exerts primary control on regional groundwater resources in aquifers hosted in primarily volcanic geologic settings. New geologic maps, topographic analysis, airborne thermal infrared (TIR) remote sensing data on stream temperature, and streamflow data are combined to gain insight into the surface-water and groundwater systems of the understudied Hat Creek basin, which sits within the Hat Creek focus area (Fig. 2). Together, the structure and stratigraphy, the three-dimensional (3D) conceptual model, and the locations of surface-water/groundwater interactions all help identify the potential structural or stratigraphic factors that influence streamflow gains and losses.

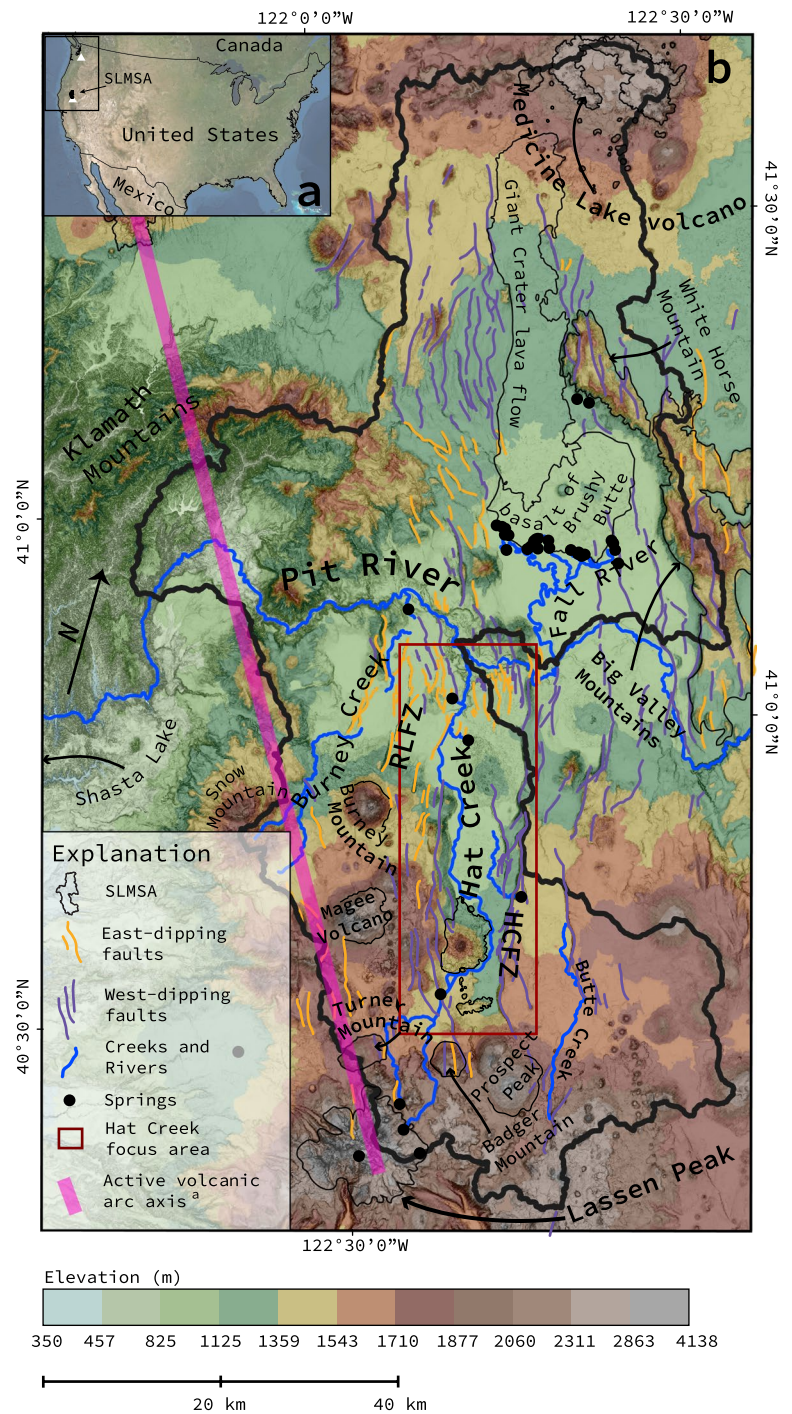
The Hat Creek basin is a major year-round, groundwater-fed contributor to the Pit River and Shasta Lake. However, the heterogeneity of volcanic deposits, sampled at very few wells in only a small part of the basin, makes study of this system challenging, and many of the common hydrogeology tools (such as potentiometric surface maps) are unavailable. Instead, the conceptual model of the groundwater basin is developed to be consistent with volcanic aquifer studies elsewhere (Lindholm 1996; Gingerich 1999; Gannett et al. 2001, 2007; Burns et al. 2011). The conceptual model is then constrained with available water-well data, geologic maps, and comparatively high-resolution streamflow and temperature surveys.

Background and methods

Background: translating volcanic geology to hydrogeology

The relationship between volcanogenic landforms and hydrogeology coupled with the plate tectonic setting, precipitation patterns, and previous research influence the understanding of the relationship between the geology and hydrology of the SLMSA. Grouping volcanic units by lava-flow geochemistry, cooling history, and geomorphic form and age and (or) alteration (sections 'Lava-flow geochemistry, cooling, and geomorphic form' and 'Hydrogeologic implications of lava-flow geochemistry, cooling, and geomorphic form'), allows for a broad classification of water-bearing units (section 'Hydrogeologic units'). This section, 'Background: translating volcanic geology to hydrogeology', and its subsections, lay the conceptual groundwork for volcanic hydrogeology in the Cascade Range of northern California, leading into sections 'Geology and hydrology of the Hat Creek basin' and 'Methods of hydrogeologic analysis'.

Fig. 1 **a** Location map with two white triangles representing Mount Rainier (north) and Lassen Peak (south) and **b** elevation map of Shasta-Lassen Peak-Medicine Lake volcano study area (SLMSA) and the Hat Creek focus area (red box). Elevation mapped on slope-shaded relief includes labels (HCFZ: Hat Creek fault zone, RLFZ: Rocky Ledge fault zone) for topographic features, east-dipping and west-dipping faults and streams and rivers. Legend footnote: ^aModified from Wells and McCaffrey (2013)



Geographic setting

The SLMSA lies between Medicine Lake volcano to the north, Lassen Peak to the south, the Big Valley Mountains

to the east and Mount Shasta to the northwest (Fig. 2). The Pit River bisects the SLMSA and gains water from the Fall River to the north and Hat Creek and Burney Creek to the south before draining into Shasta Lake to the west (Fig. 2).

Fig. 2 Average annual precipitation (1981–2010, PRISM Climate Group 2015) mapped on a slope-shaded relief map of the Shasta-Lassen Peak-Medicine Lake volcano study area (SLMSA) with rivers and high-volume springs. The highest amounts of precipitation fall on the high elevations (Fig. 1b) near the volcanic-arc axis, including Lassen Peak to the south and Mount Shasta. East of the axis of the Cascade Range, higher precipitation occurs at the relatively higher elevation peaks such as Medicine Lake volcano. The SLMSA polygon is restricted to the region that provides groundwater to the high-volume springs. The green box identifies precipitation pixels at higher elevations than Big Spring. The yellow box identifies the precipitation pixels around Magee Volcano

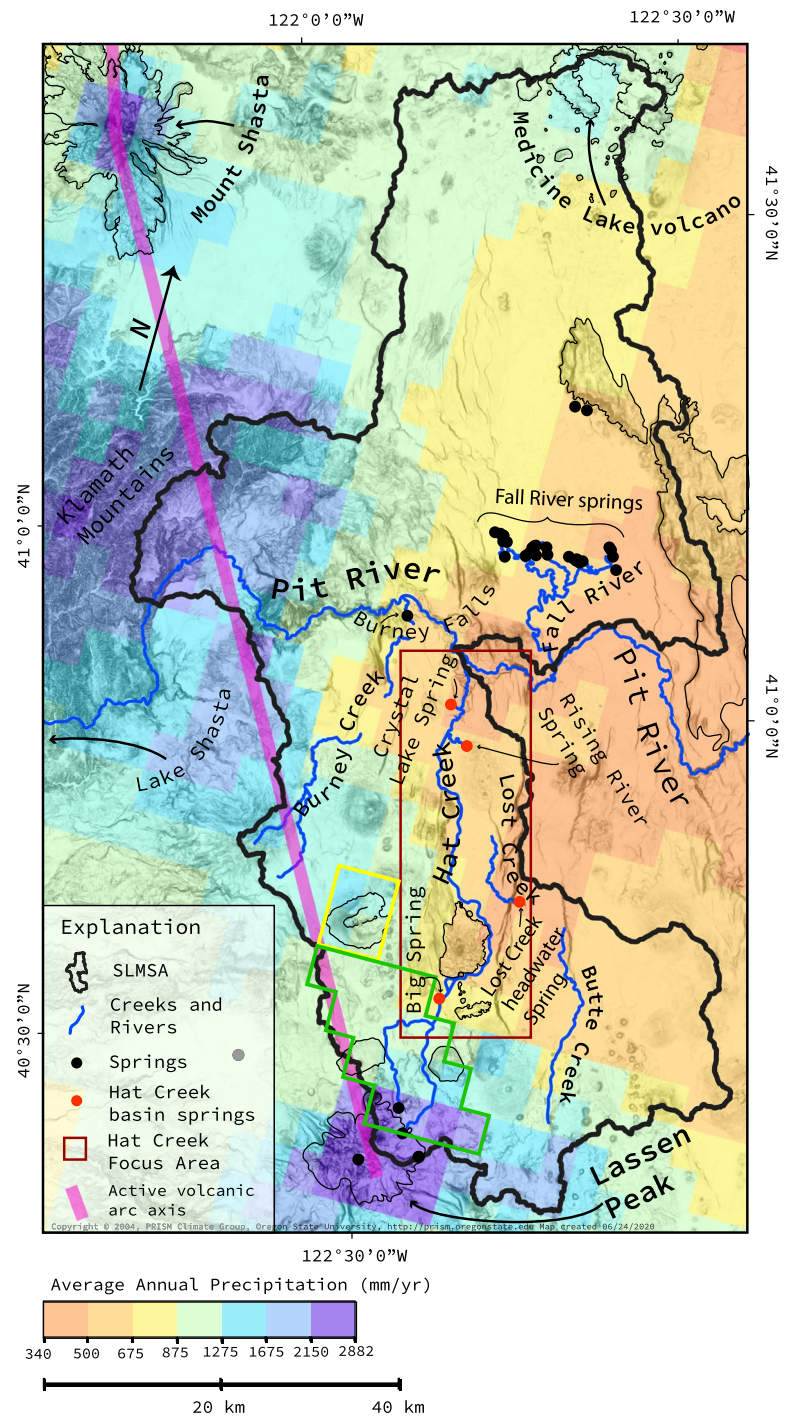


Plate tectonic setting

The SLMSA spans the northwestern section of the Basin and Range Province, the southern end of the Cascadia subduction zone and related Cascades Volcanic Arc, and the northwestern edge of the Walker Lane Fault Zone (Fig. 3a;

Blakely et al. 1997; Langenheim et al. 2016). Reorganization of the Pacific–North American plate boundary at about 30 Ma preceded Basin and Range extension (Atwater 1970; McQuarrie and Wernicke 2005; Wesnousky 2005a; Colgan et al. 2006). The Walker Lane Fault Zone, a NW–SE trending ~120-km-long belt of right-lateral shear, accommodates up to

20–25% of the movement between the Pacific-North America plate boundary (Blakely et al. 1997; McQuarrie and Wernicke 2005; Wesnousky 2005b; Lee et al. 2009). Cascades arc volcanism and Basin and Range low-volume extensional volcanism both use N–S and NW–SE striking faults as magma conduits between melt sources and the surface (Muffler et al. 2011; Muffler and Clynne 2015). Normal and dextral-oblique faults are responsible for regional Crustal deformation; these normal fault-related basins and ranges reflect the dominant-structural expression in the regional topography (Blakely et al. 1997; Unruh and Humphrey 2017).

Precipitation

The Cascade Range orographic effect causes a rapid decline in average annual precipitation with distance east from the active axis of the Cascade Range (Fig. 2). However, Medicine Lake Volcano, and some other high-elevation areas east of the active volcanic arc axis (Fig. 2), receive relatively high average-annual precipitation (>1,000 mm/year; Figs. 1 and 2; PRISM Climate Group 2015).

Previous work within the SLMSA

Most past hydrogeologic studies in SLMSA focused on geochemically identifying potential groundwater-recharge locations (Rose et al. 1996; Davisson and Rose 1997, 2014), sources of groundwater discharge into streams (Davisson and Rose 2014), and heat and fluid flow in the Medicine Lake Volcano-Fall River system (Burns et al. 2017b). Isotopic data indicate that water sourced from Lassen Peak and some adjacent volcanic peaks contributes to the Hat Creek springs (Rose et al. 1996; Fig. 1). Burns et al. (2017b) built upon the foundational work of Rose et al. (1996), Davisson and Rose (1997, 2014), and Manga and Kirchner (2004) to study the relationship between climate, spring discharge, and temperature at Fall River springs (Fig. 3). Burns et al. (2017b) found that both precipitation (in excess of 700 mm/year), recharge temperatures, and decadal-scale changing atmospheric temperatures affect spring temperatures, but that characteristics of the groundwater system, such as the vadose zone's ability to thermally insulate the aquifer, buffer spring temperature changes. Building on previous work (Rose et al. 1996; Davisson and Rose 1997; Manga and Kirchner 2004; Davisson and Rose 2014), Burns et al. (2017b) concluded that changes in spring temperature will lag changes in climate by tens to hundreds of years.

Previous work quantifies the general nature of groundwater/surface-water exchange in the SLMSA. Generally, both groundwater and surface-water flow from the topographically elevated, high-precipitation uplands toward the Pit River (Figs. 1 and 2). In the morphologically similar upper Deschutes River basin (an eastside Cascade Range drainage

basin north of the SLMSA), highly permeable younger volcanic rocks form productive aquifers that often discharge at high-volume springs where young volcanic units onlap older less-permeable rocks (Gannett et al. 2001). In the Hat Creek basin, large volume springs are observed to discharge from similarly young volcanic rock.

Lava-flow geochemistry, cooling, and geomorphic form

In the SLMSA, a primarily volcanic region with occasional sedimentary interbeds, volcanic units can be differentiated by geochemistry and landform (Fig. 3c). Geochemical groups are (1) calc-alkaline rocks or (2) low-potassium olivine tholeiite rocks. Calc-alkaline magmas, linked to arc volcanism, have high viscosity (Manga 1997; Lyle 2000; Manga 2001; Harris 2013; Muffler and Clynne 2015; Clynne and Muffler 2017; Fig. 3) and form scoria cones, steep-sided lava cones and broad shield volcanos, all with high aspect ratios and limited lateral extents (Clynne and Muffler 2010; Muffler and Clynne 2015; Clynne and Muffler 2017). Low-potassium olivine tholeiite magmas, associated with crustal extension, have low viscosity and produce widespread low-relief, valley-filling, sheet-flows from low, commonly inconspicuous vents (Fig. 3; Clynne and Muffler 2010; Muffler and Clynne 2015; Clynne and Muffler 2017). Multiple episodes of low-viscosity eruptions can create a stratigraphic sequence of stacked lava flows and sedimentary interbeds (Burns et al. 2011).

Cooling forms many of the primary geomorphic features and textures found in calc-alkaline and low-potassium olivine tholeiite rocks. Textures found in lava flow tops and bottoms include interconnected vesicles and cracks and are generated by a range of processes, including cooled rubble pushed forward and overridden as the lava flows, boiling water in soil, or degassing of the lava flow (Manga 2001). Lava-flow interiors also display a range of cooling textures but are often dense, possibly with cooling joints (Grossenbacher and McDuffie 1995; Lyle 2000). Shields, scoria cones, and lava cones tend to have pervasive, randomly oriented fractures produced during and after emplacement (Pollard and Aydin 1988; Grossenbacher and McDuffie 1995; Kattenhorn and Schaefer 2008).

Hydrogeologic implications of lava-flow geochemistry, cooling, and geomorphic form

Morphological features, like lava-flow tops (Manga 2001) and age-related features, such as secondary mineralization (Jefferson et al. 2010; Burns et al. 2017a), influence groundwater flow in volcanic systems. Porous and permeable lava-flow tops, bottoms, and interflow zones (where one lava-flow top meets the overlying lava-flow bottom) often serve as the primary horizontal fluid-flow media in volcanic aquifers (Gannett et al. 2001; Manga 2001; Burns et al. 2012, 2016).

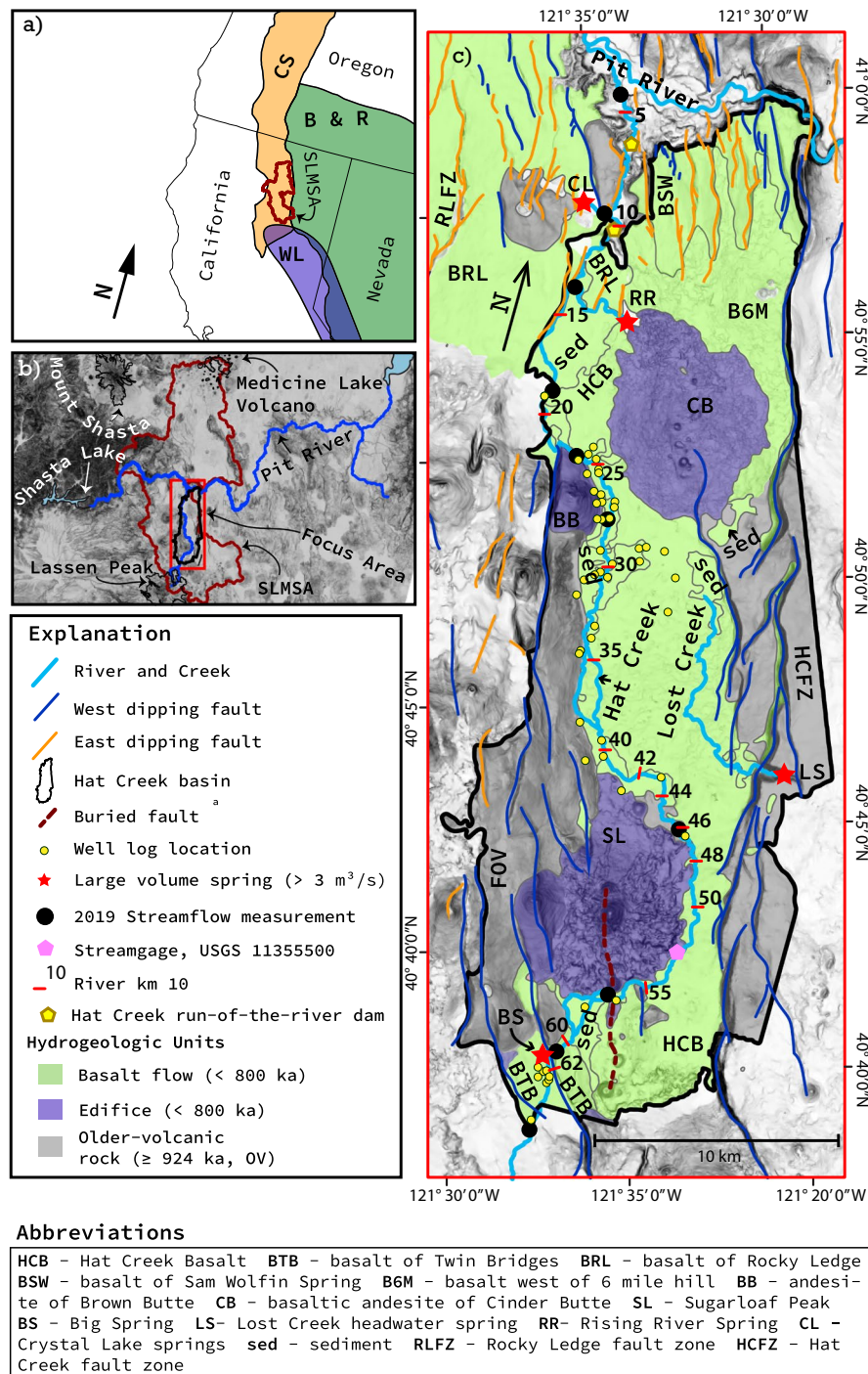


Fig. 3 Geology of the Hat Creek focus area. **a** The Basin and Range extensional province (B&R), Cascade Range (CS), and Walker Lane Fault Zone (WL) intersect in the Shasta-Lassen Peak-Medicine Lake volcano study area (SLMSA, red/brown outline). Modified from Langenheim et al. (2016) and from US Geological Survey physiographic divisions of conterminous USA (Fenneman and Johnson 1946). **b** Geographic setting of SLMSA and the Pit River drainage basin. Red box indicates the location of the Hat Creek focus area (c). **c** Conceptual geologic map of the Hat Creek focus area. Volcanic rocks are grouped

into three units. Green identifies basalt flows and Holocene sediments. Purple area depicts high-elevation volcanic edifices. Faulted-older-volcanic units that form the valley and are exposed in adjacent uplands are in gray. Informal names of volcanic units are based on Muffler and Clynne 2015. Labels include HCFZ: Hat Creek fault zone, RLFZ: Rocky Ledge fault zone. Fault dip direction was established with a LiDAR-derived slope shade map, US Geological Survey Quaternary Fault and Fold Database of the United States (US Geological Survey 2018), and geologic mapping. Legend footnote: ^aClynne and Muffler (2017)

Extensive jointing can serve as a mechanism to explain vertical connectivity between volcanic aquifers (Gingerich 1999; Davissou and Rose 2014), although closed fractures—such as cooling joints under confining pressure—unconnected fractures, or fractures filled with alteration minerals often prevent vertical fluid flow (Burns et al. 2016). The amount of alteration minerals plugging groundwater flow paths increases over time, and temperatures >30–45 °C accelerate the rate of alteration (Burns et al. 2012, 2015, 2016, 2017a). As a result, permeability generally decreases with geologic age (Gannett et al. 2001; Jefferson et al. 2010; Burns et al. 2017a). The relationship between permeability and age of volcanic terranes determines river and stream drainage density (Jefferson et al. 2010) and spring density (Burns et al. 2017a). Young, high-elevation volcanic features may be permeable and allow rapid groundwater recharge from rain and snowmelt (Jefferson et al. 2010; Burns et al. 2017a).

The hydrologic implications of age and morphology of volcanic units serve to differentiate and characterize the basin-filling units in the Hat Creek focus area (Figs. 3 and 4). Geochemistry can determine the extent of a volcanic unit as either extensive or limited. The morphology, controlled by the geochemistry of the units, can determine where water can flow within them; that is, horizontally at flow tops, bottoms, and interflow zones and/or vertically through fractures. Alteration of volcanic glass to pore-filling clays increases with age and may limit fluid flow through volcanic media. However, the 124-ka age difference between the basin-forming unit and the oldest basin filling unit (Table 1; Fig. 3) might not substantially affect the permeability of the rocks. Thus, rocks in the study area might not be old enough for extensive alteration to have taken place. Instead, basin-bounding structures, like the Hat Creek fault zone (HCFZ, Fig. 1), separate and differentiate younger-basin-filling rocks from the adjacent older-volcanic uplands.

Geology and hydrology of the Hat Creek basin

Conceptual model of groundwater flow

In the conceptual model of groundwater flow for the Hat Creek basin, young, permeable, laterally connected, basin-filling basalt flows in the valley bottom accumulate water from the adjacent and southern uplands. These young basalt flows efficiently transmit water from Lassen Peak to the south to the Pit River to the north. Geologic structure in the valley controls both the space the young basin-filling-basalts fill and the degree of tilting they undergo. The volcanic history is important because age and deposition control the way volcanic units interact with the groundwater system (sections ‘Lava-flow geochemistry, cooling, and geomorphic form’ and ‘Hydrogeologic implications of lava-flow geochemistry,

cooling, and geomorphic form’). Oxygen isotopes enable the identification of apparent recharge elevation. This information enables the construction of a 3D hydrogeologic model of the Hat Creek basin consistent with the broader understanding of the hydrogeology of the volcanogenic terranes.

Geologic structure

Faulting plays two key roles in the geologic evolution of the Hat Creek basin (Fig. 3) by (1) determining the shape of the basin and (2) controlling the source and extent of volcanic units deposited within the basin (Leeder and Gawthorpe 1987; Gawthorpe and Leeder 2000). From south to north, fault dips change from predominantly down-to-the-west (Anderson 1940; Muffler et al. 1994; Langenheim et al. 2016) to east dipping on the west side of the basin and west dipping on the east side (Austin 2013, Figs. 1 and 3). The HCFZ runs for 47 km along the eastern margin of the Hat Creek basin, has a maximum vertical displacement of 370 m (Anderson 1940; Muffler et al. 1994; Blakeslee and Kattenhorn 2013; Kattenhorn et al. 2016) and controls the basin’s geometry (Langenheim et al. 2016; Fig. 3). Crustal-scale faults can act as pathways for the vertical migration of magmas (Le Corvec et al. 2013; Muffler and Clyne 2015; Clyne and Muffler 2017) and might collocate volcanic centers, like Sugarloaf Peak and Cinder Butte, with fault traces.

Previous geologic work suggests two structural models for the Hat Creek basin: full graben and half graben. In the first model, the basin is envisioned as a full graben bounded by the HCFZ to the east and the Rocky Ledge fault zone (RLFZ) and associated faults to the west (Austin 2013; Fig. 1). In the second model, a half-graben with most displacement on the HCFZ is proposed. Principal evidence for the second model includes the asymmetric geometry of the basin (Muffler et al. 1994), east-tilting volcanic and volcanoclastic units (Anderson 1940; Kattenhorn et al. 2016), and the eastward thickening of valley fill (Langenheim et al. 2016).

The structural model for extension changes from south to north in the Hat Creek basin. The HCFZ (maximum age of 924 ka, Clyne and Muffler 2010; Kattenhorn et al. 2016) dips to the west, provides the most relief in the focus area, and creates accommodation space by separating the valley bottom from adjacent uplifted fault-blocks to the east (Fig. 3; Anderson 1940; Muffler et al. 1994; Blakeslee and Kattenhorn 2013; Kattenhorn et al. 2016). On the southwestern side of Hat Creek focus area, an unnamed fault collocated with Big Spring also dips to the west (Fig. 3). To the northwest of Brown Butte, the east-dipping RLFZ accommodates strain on the western margin of the basin, while the HCFZ maintains strain accommodation on the east (Anderson 1940; Austin 2013; Fig. 1).

Volcanic history

Volcanic units in the Hat Creek focus area are basin-filling rock units (<800 ka) and are younger than the basin-forming, faulted older volcanic (>924 ka) rocks, that underlie the valley bottom and bound the basin to the east and west (Table 1). Rocks in the Hat Creek basin are volcanic unless stated otherwise. The most well-constrained basalt flow in the Hat Creek basin is the Hat Creek Basalt (HCB), which is 30 m thick on its eastern margin and thins to 0 m thick on its western margin.

Isotope data and apparent recharge elevation

Recharge elevations for springs feeding Hat Creek were estimated by Rose et al. (1996) and Davisson and Rose (1997), using $\delta^{18}\text{O}$ isotopes and were used to identify volcanic peaks that serve as possible water sources (Rose et al. 1996; Davisson and Rose 1997). Relatively low $\delta^{18}\text{O}$ values at Big Spring indicate a flow-weighted average elevation matching Crater Peak on Magee Volcano (Rose et al. 1996), although this elevation could also represent the average of a range of elevations from Lassen Peak to Badger Mountain (Fig. 1). Rising River springs and Crystal Lake springs discharge water matching a flow-weighted average elevation from the high-elevation, high-precipitation region near Lassen Peak (Figs. 1 and 2; Rose et al. 1996; Davisson and Rose 1997).

Methods of hydrogeologic analysis

The volcanic history with geologic mapping and the structural history were used to characterize geologic units into hydrogeologic units based on concepts from section ‘Hydrogeologic implications of lava-flow geochemistry, cooling, and geomorphic form’. Basalt-flow-unit tops and bases were interpolated for a limited area south of Cinder Butte using interpreted well-log geologic contacts to estimate the location and dip of lava-interflows (potential aquifers) in the subsurface (available well logs shown on Fig. 3). Late-summer

streamflow measurements paired with stream-temperature estimates from an airborne thermal infrared remote-sensing (TIR) survey were used to estimate locations and magnitude of stream gains and losses from stream confluences and to and from the groundwater system. Overlaying gains and losses onto hydrogeology allows the identification of geologic controls on groundwater flow.

Thematic geologic maps

Geologic maps were constructed to separate volcanic units into basin-forming (>924 ka) and basin-filling (<800 ka) basalt flows and volcanic edifices using geologic mapping and age data (Gay and Aune 1958; Lyden et al. 1960; Muffler et al. 1994; Clynne and Muffler 2010; Downs et al. 2020), 1/3 arc second LiDAR digital elevation models (DEM, US Geological Survey 2019b), and the US Geological Survey active faults database (US Geological Survey and California Geological Survey 2018). Once geologic maps and US Geological Survey Quaternary fault and fold database were integrated with LiDAR, a few new faults were identified based on aspect and slope angle. Using the DEM (US Geological Survey 2019b), topographic scarps with slopes >25° were identified as faults.

Hydrogeologic units

The depositional volcanic-rock units were categorized into hydrogeologic units based on composition, morphology, and age/degree of faulting. The subdivisions are basin-filling (<800 ka), consisting both of volcanoes and lava flows, and the faulted, basin-forming (>924 ka) volcanic unit (Older Volcanic units, OV). These age distinctions were designed to differentiate units younger than the basalt of Twin Bridges (BTB, Tables 1 and 2) from those older than the initiation of faulting on the HCFZ. Young volcanic rocks will henceforth be referred to as ‘basin-filling’ and are further subdivided into edifice aquifers and basalt-flow aquifers (Fig. 4). The conceptualized basalt-flow aquifers have the potential

Table 1 Basin-filling rocks of the Hat Creek focus area

Abbreviation	Name	Age \pm error (ka)	Composition
HCB	Hat Creek Basalt	24 \pm 6 ^b	Basalt
CB	Cinder Butte	38 \pm 7 ^b	Basaltic andesite
SL	Sugarloaf Volcanic Chain	46 – 77 \pm 7, 11 ^b	Andesite and basaltic andesite
B6M	Basalt west of Six Mile Hill	53.5 \pm 2 ^d	Basalt
BRL	Basalt of Rocky Ledge	200 \pm 8 ^c	Basalt
BSW	Basalt of Sam Wolfen Spring	647.3 \pm 21.7 ^d	Basalt
BTB	Basalt of Twin Bridges	730 – 780 ^a	Basalt
BB	Brown Butte	NA	Andesite

^aClynne and Muffler (2010), ^bTurrin et al. (2007), ^cClynne and Muffler (2017), ^dMuffler and Clynne 2015

Table 2 Volcanic units in the Hat Creek basin study area and corresponding hydrogeologic units

Abbreviation	Name	Age \pm error (ka)	Composition	Hydrogeologic unit
HCB	Hat Creek Basalt	24 ± 6^b	Basalt	Basalt-flow aquifer
CB	Cinder Butte	38 ± 7^b	Basaltic andesite	Edifice aquifer
SL	Sugarloaf Volcanic Chain	$46 - 77 \pm 7, 11^b$	Andesite and basaltic andesite	Edifice aquifer
B6M	Basalt west of Six Mile Hill	53.5 ± 2^d	Basalt	Basalt-flow aquifer
BRL	Basalt of Rocky Ledge	200 ± 8^c	Basalt	Basalt-flow aquifer
BSW	Basalt of Sam Wolfen Spring	647.3 ± 21.7^d	Basalt	Basalt-flow aquifer
BTB	Basalt of Twin Bridges	$730 - 780^a$	Basalt	Basalt-flow aquifer
BB	Brown Butte	NA	Andesite	Edifice aquifer

^aClynne and Muffler (2010), ^bTurrin et al. (2007), ^cClynne and Muffler (2017), ^dMuffler and Clynne 2015

to form laterally extensive aquifers (Gannett et al. 2001; Manga 2001; Burns et al. 2012, 2016; Figs. 4 and 5c). The Hat Creek Basalt (HCB), BTB, the basalt of Rocky Ledge, the basalt of Sam Wolfen Spring, and the basalt west of Six Mile Hill are the only mapped basin-filling units that may form basalt-flow aquifers within the study area (Table 2). Edifice-aquifer units allow efficient recharge and may be hydraulically connected (Pollard and Aydin 1988) to multiple basalt flow aquifer units via onlap and/or fault-controlled contacts (Figs. 4 and 5). OV units underlie basin filling units and form the adjacent uplands. Whereas basin-filling laterally extensive low-permeability basalt-flow interiors likely minimize hydrologic exchange with OV units beneath the valley bottom, there is the potential for groundwater to flow from the adjacent uplands as springs or possibly laterally into lowland aquifers via highly heterogeneous flow paths (sections ‘Hydrogeologic implications of lava-flow geochemistry, cooling, and geomorphic form’ and ‘Geologic structure’). High amounts of faulting in OV, compared with the basin-filling unit, serve as its main distinction, as offsets can form barriers to groundwater flow through thin volcanic aquifers (Figs. 4 and 5).

The morphology of lava flows in the Hat Creek basin is highly variable; but can be conceptualized as having a dense (low porosity and permeability) flow interior, and porous and permeable flow tops and bottoms that cooled rapidly (see sections ‘Lava-flow geochemistry, cooling, and geomorphic form’ and ‘Hydrogeologic implications of lava-flow geochemistry, cooling, and geomorphic form’). Permeability within interflow zones (a lava flow top, possibly overlain with a sedimentary interbed, and the overlying lava flow bottom) can result from a wide range of processes during lava flow deposition (see sections ‘Lava-flow geochemistry, cooling, and geomorphic form’ and ‘Hydrogeologic implications of lava-flow geochemistry, cooling, and geomorphic form’). For Columbia River basalts, permeable thickness is estimated to be 1/10 of total thickness on average (Burns et al. 2011), but insufficient data exist to give a typical ratio for Hat Creek area valley-filling basalts. Faults can act as

barriers to lateral flow when permeable interflow zones become juxtaposed with low permeability flow interiors, and fault permeability (dominated by previously unaltered flow interiors) decreases over time as fault gouge alters to clays.

In the Hat Creek basin, the maximum exposed thickness of the basin-filling BTB unit is around 30 m (at the fault at Big Spring, Fig. 3), though most of the thin flows are tens of centimeters to a few meters thick (Clynne and Muffler 2010) and the maximum expression of the Hat Creek Basalt is at least 30 m on the east side of the valley, though it could be thicker. The greatest amount of vertical displacement on the Hat Creek fault zone is 370 m, though this represents an underestimate of vertical movement on the fault as younger lava flows partially cover older scarps (Anderson 1940; Muffler et al. 1994; Blakeslee and Kattenhorn 2013; Kattenhorn et al. 2016). This means that even though the OV unit can transmit water (e.g., Lost Creek headwater spring, Fig. 3), it is assumed to be a separate hydrogeologic unit, particularly because Lost Creek headwater spring discharges above the Hat Creek Valley bottom, implying a separate, higher-elevation aquifer with markedly different hydraulic head.

Well log analysis

Water-well logs (Fig. 3; Marcelli and Peterson 2022) are used to estimate the dip and thickness of basin-filling basalts. Identifying points at potential stratigraphic contacts allows for the construction of contact-trend surfaces that estimate locations for the top and bottom of each unit (i.e., potential aquifers). The elevation of each stratigraphic contact is estimated from water-well logs (Marcelli and Peterson 2022), mapped surficial geology and the DEM (US Geological Survey 2019b). Only the general dip directions and dip angle are used herein to develop the conceptual hydrogeologic framework. In order to achieve a smooth surface, each contact-trend surface was estimated using LOESS (Cleveland 1979). Additionally, the mapped extent of the exposed parts of the HCB and the BTB was used in conjunction with stratigraphic contacts found in well logs to generate estimates for HCB top and BTB top.

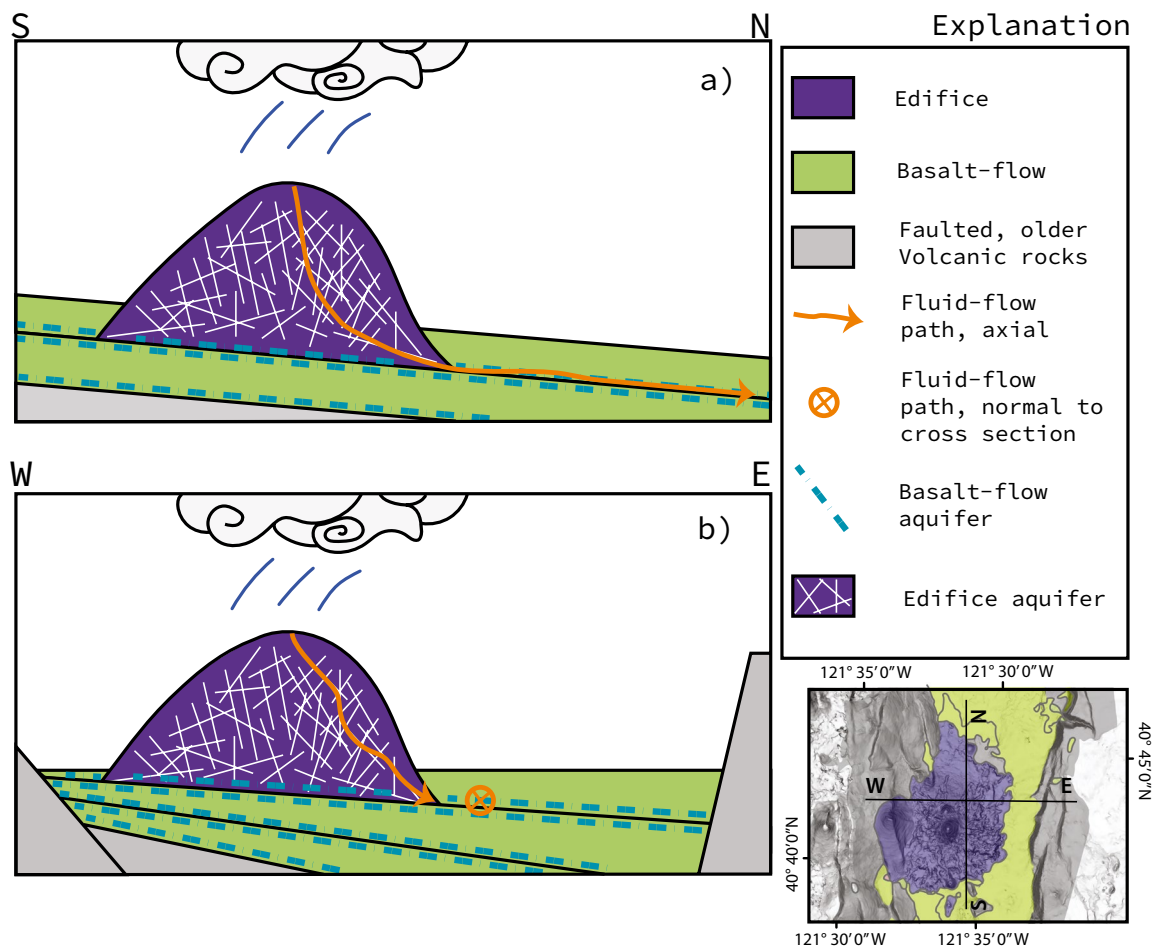


Fig. 4 The three main hydrogeologic units in the Hat Creek basin depicted **a** along the valley axis and **b** across the valley. Groundwater flows downslope (S–N). Basalt-flow aquifers (<800 ka) have primary permeability structures that consist of lava tubes and the intraflow breccia, sediments and interconnected vesicles found at lava-flow tops and bottoms. Undeformed basalt-flow aquifers efficiently transmit water downvalley, but upflow from underlying units is inhibited. Transport distance depends on the extent and interconnectivity of the basin-filling rocks. Edifice aquifers, formed by emplacement of calc-

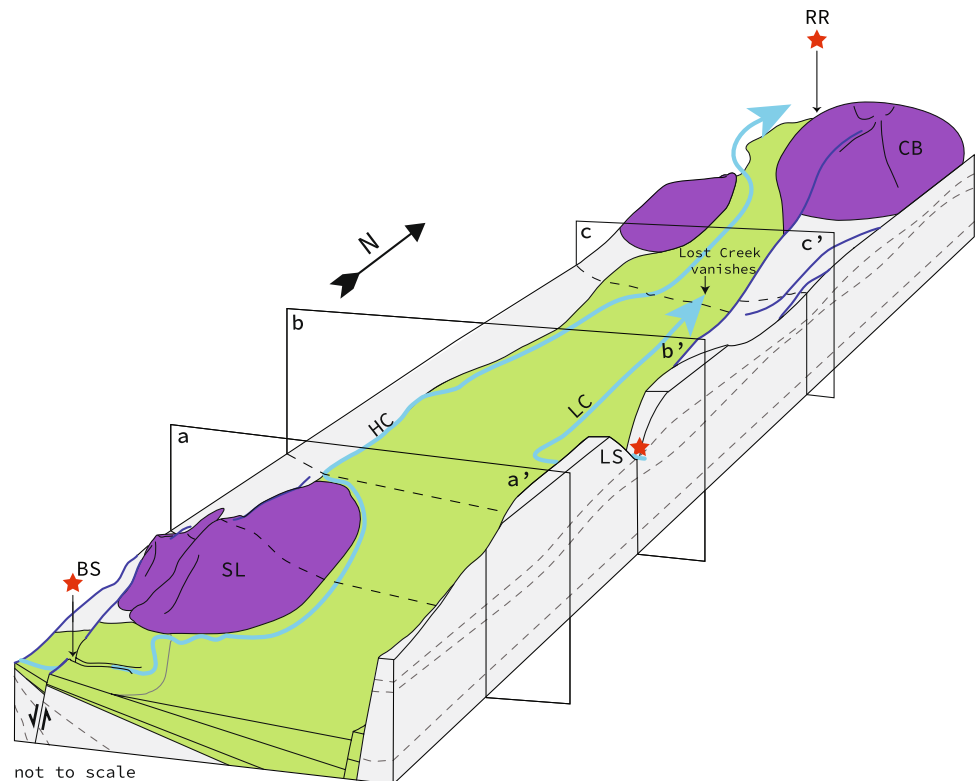
alkaline magmas, have permeability structures that consist of porous volcanic deposits and pervasive, randomly oriented fractures. They have limited extent, but are often very permeable, allowing easy vertical movement of water into the aquifer system. The OV unit (≥ 924 ka) underlies and contains the basin-filling basalt-flow and the edifice aquifers. The fluid-flow path normal to the cross section points away, in the downstream direction (north). The inset depicts the locations of the conceptual cross sections running through Sugarloaf Peak (labeled S–N or W–E accordingly)

Streamflow measurements

Daily streamflow at the Hat Creek streamgage (US Geological Survey station 11355500, Fig. 3c) and late-season (September 8–19, 2019) streamflow measurements along Hat Creek (Fig. 3c) are used to identify temporal and spatial patterns in groundwater discharge along Hat Creek in 2019. A late-summer seepage run (following a 2018 airborne stream temperature survey [section [Airborne thermal infrared remote sensing of stream temperature](#)]) targeted streamflow measurements were collected over the length of the stream for the purposes of estimating locations and rates

of groundwater discharge and infiltration) from September 8 to 19, 2019 (Fig. 3; US Geological Survey 2019a). Summer low-flow estimates (i.e., groundwater dominated) at the US Geological Survey Hat Creek stream streamgage from 1928–2000 and 2015–2019 are used to identify groundwater discharge variability in the Hat Creek over a range of years and climate conditions (US Geological Survey 2019a). Characterization of temporal variability in streamflow along Hat Creek is provided by additional dry-season measurements at a range of locations during the years 1912, 1921, 1922, 1928, 1988, 2002, 2015, 2016, and 2017 (US Geological Survey 2019a). The measurements were taken during late summer

Fig. 5 Conceptual 3D diagram of the hydrogeologic organization of the Hat Creek basin. Stacked laterally hydraulically- and physically connected basalt-flow aquifers (green) are found at the contacts between individual basalt flows and transmit water horizontally. Edifice aquifers (purple) provide efficient recharge and vertical connectivity through high elevation peaks, and are connected to the OV unit (gray) and younger aquifers in complex ways due to heterogeneity and faulting. Dashed lines in the OV represent older tilted depositional units. Arrows in the creeks indicate the surface-water flow directions. The HCB and BTB units both fall under the basalt-flow aquifer category, though three units are depicted here to illustrate the point. Locations of sections in Fig. 6 are shown here



Abbreviation

HC-Hat Creek	LS- Lost Creek headwater springs	SL-Sugarloaf Peak
CB-Cinder Butte	LC-Lost Creek	BS-Big Spring
		RR- Rising River Spring

when precipitation and surface runoff are lowest. Though late-summer evapotranspiration is at its highest, for analyses herein, evapotranspiration and precipitation are assumed to be negligible compared to other inflows and outflows. This enables the assumption that all measured gains and losses from the surface-water system comes from interaction with groundwater, tributaries, or dam operations (including diversions and return flow).

Airborne thermal infrared remote sensing of stream temperature

Spatial variation of water temperature in rivers is influenced by atmospheric heat exchange, topography and geographic setting (e.g., shade and albedo), streamflow (thermal inertia), hyporheic exchange, tributary inflow, and exchange of water with the aquifer system. Determining the relative influences of these variables is challenging because more than one process may be occurring along any given stream reach (Caissie 2006). TIR remote sensing can detect the effects of

groundwater discharge on water temperature along the stream length. Inputs of relatively cool water create both discontinuities (e.g., cooling over a short reach) and anomalous departures from the expected longitudinal warming pattern in the downstream direction (e.g., cooling due to diffuse groundwater discharge; Fullerton et al. 2015). When thermal anomalies cannot be explained by surficial atmospheric, topographic, or advective drivers (e.g., tributary inflows), the longitudinal profile of stream temperature provides an indirect method to identify the locations and relative magnitude of groundwater/surface-water exchange (Dugdale et al. 2015).

Several studies have used TIR data to identify hydromorphologic and landscape features such as channel curvature and confinement, slope, valley morphology and geology associated with cold-water areas (Loheide and Gorelick 2006; Monk et al. 2013; Dugdale et al. 2015; Casas-Mulet et al. 2020). Recent approaches employ modeling in tandem with TIR data to disentangle the multiple effects of hydrologic, geomorphic, topographic, and geologic factors on longitudinal variability in stream temperature (O'Sullivan et al. 2019, 2020). Geologic

setting and associated structure and lithology can be important drivers of longitudinal variation in stream temperature. Detailed high-resolution geologic maps of rivers with TIR data are needed to link the vertical dimension of hydrogeology with thermal heterogeneity in riverscapes (Fullerton et al. 2015; O'Sullivan et al. 2020).

In 2018, airborne TIR surveys (using the methodology of Torgersen et al. 2001) were conducted in the afternoon (4:37–7:00 pm) and morning (7:05–9:22 am) of both September 24 and 25 to measure water-surface temperature of the lower 65 km of Hat Creek. In rivers with no interaction with groundwater, radiant temperatures should rise steadily through the day and with distance from the source (Fullerton et al. 2015). Comparing radiant temperatures from the morning and afternoon allows spatial characterization of similar anomalous low or high temperatures along reaches of a stream, identifying locations of groundwater/surface-water interaction. Detailed descriptions of TIR methods, imagery, and data are provided by Curtis et al. (2021). The morning and afternoon surveys were conducted using a helicopter-mounted forward-looking infrared (FLIR) SC6000 LWIR sensor (FLIR Systems, Inc.) flown 300–400 m above Hat Creek. The sensor measured wavelengths of 8–9.2 μm . Twelve digital temperature loggers (HOBO Water Temperature Pro v2 Data Logger, U22-001; Onset, Inc.) distributed within the flowing stream along Hat Creek were used to calibrate radiant temperatures in the thermal imagery. TIR temperatures were within 0.5° of in-stream temperatures (Curtis et al. 2021). Typically, channel width exceeds 4 m for the surveyed reaches, so the channel was adequately sampled by the georeferenced TIR image mosaics that have a spatial resolution of $0.5\text{ m} \times 0.5\text{ m}$. The thalweg path was digitized manually and did not vary at the channel unit scale (e.g., riffles, $\sim 10\text{ m}$). To remove numerical artifacts in estimated stream temperature, median temperature along each 10 m length was used. Where the median temperature picks did not correspond with the stream channel, median temp picks were removed. A gap of 400 m exists upstream of the confluence with Rising River, where low flow conditions and narrow channel made choosing a thalweg from the TIR data difficult (Fig. 3). Median temperatures were plotted longitudinally with respect to the distance upstream ('river km') from the mouth of Hat Creek where it enters the Pit River.

Results of hydrogeologic analysis

The mapped depositional units, used to create the hydrogeologic units, and stratigraphic trends calculated from geologic contacts found in well logs are used to create a 3D conceptual representation of the focus area groundwater system (Fig. 5). Measured streamflow, stream temperature, and flow

from springs can be compared to average creek conditions to analyze surface-water/groundwater interactions.

Structure and stratigraphy

Depositional horizons identified in well logs generally dip and units thicken to the north or northeast (Fig. 5). These trends are due to both the geometry of the basin in the south (east dipping half-graben where the basin is surrounded by west-dipping faults, Fig. 3, section 'Conceptual model of groundwater flow') and the general topographic trend (elevation decreases with distance from Lassen Peak, Fig. 1). The maximum exposed extent of the HCB on the eastern side of the valley is 30 m, and it thins to 0 m on the western margin of the valley, but due to the sparse water-well logs (Fig. 3), much of the subsurface geometry of the basalt is unconstrained. The HCB forms much of the valley floor of the Hat Creek basin. Surfaces created by LOESS over the water-well log (Fig. 3) contacts (section 'Well log analysis') vary in space, allowing estimation of variations in dip direction and dip (Table 3). These surfaces are used to conceptualize the geometry of the Hat Creek basin for the conceptual model (section 'Hydrogeologic units'). The Hat Creek basin has components of both a strong topographic dip (north) and a structural dip (east/northeast), with buried basalt flows thickening and contacts generally dipping in these directions.

Both HCB top and HCB bottom have north to north–northeast dip directions and similar dip angles (Table 3), and slightly thicken to the northeast. The upper trend surface for the basalt of Twin Bridges has dip directions clustered between northeast and east and dips centered on 2.2° , but that range between 1.4 and 12° (Table 3). Both HCB top and HCB bottom dip to the north rather than the east–northeast, as BTB top does. HCB bottom's max dip (1.48°) and BTB top's minimum dip (1.4°) have a $.08^\circ$ difference implying that they could sequentially stack atop one another. However, the difference between the BTB's maximum dip (12°), and the max dip direction (80°), and the HCB bottom's max dip (1.48°) and the max dip direction (10°) imply the existence of a unit between them. One reason maximum dips and dip directions may differ between BTB top and the two HCB contacts is a series of discontinuous sedimentary interbeds. However, there is no definitive evidence for or against the presence of a unit between HCB bottom and BTB top. The west-striking, north-dipping slopes of HCB top and HCB bottom both likely reflect the topographic dip driving the HCB's northward migration and emplacement toward the Pit River (Table 3). The BTB trend surface dips to the northeast because it is an older unit that has likely been tilted relatively more than the younger HCB; its surface reflects both the topographic trend (north dipping) and the structural trend (east dipping).

Table 3 Summary dip angle and dip direction for geologic contacts of the Hat Creek Basalt and basalt of Twin Bridges estimated from water-well logs in Hat Creek Valley

Name	Maximum dip angle (°)	Minimum dip angle (°)	Median dip angle (°)	Maximum dip direction (°)	Minimum dip direction (°)	Median dip direction (°)
Hat Creek Basalt top	1.30	0.32	1.24	020	351	014
Hat Creek Basalt bottom	1.48	1.39	1.43	010	356	357
Basalt of Twin Bridges top	12	1.4	2.17	080	025	062.5

3D conceptual model for the Hat Creek basin

Combining the thematic geologic maps (Fig. 3) with the conceptual understanding of the relationship between edifice- and basalt-aquifers (Fig. 4) and the well-log (Fig. 3) trend surfaces (Table 3) forms the basis of a 3D conceptual diagram of the hydrogeology of the focus area (Fig. 5). The conceptual hydrogeologic framework is approximate, based on geologic maps, limited water-well log data (section ‘Well log analysis’), and knowledge of regional structural geology (section ‘Conceptual model of groundwater flow’) and volcanology (section ‘Geologic structure’), and the relationship between volcanism, faulting, age (sections ‘Lava-flow geochemistry, cooling, and geomorphic form’, ‘Hydrogeologic implications of lava-flow geochemistry, cooling, and geomorphic form’ and ‘Hydrogeologic units’) and groundwater flow. Basalt-flow aquifers, at the contacts between individual basalt flows (Fig. 5), form laterally extensive aquifers that dip to the east–northeast (Table 3; Langenheim et al. 2016). Up-dip margins on the west create potential connections between the aquifers and Hat Creek (Fig. 5). Vertical hydraulic connection potentially occurs at depositional margins, contacts with edifice aquifer units, and locations where stream incisions cut through confining units. At least two basalts fill the valley (Table 3), but four hypothetical units depicted on Fig. 5 conceptually present a stack of basalt layers that interact hydrologically with each other. Figure 6b depicts a conceptual cross section from the inset Lost Creek canyon (incised by Lost Creek, flowing from a spring within the OV) on the east to the western margin of the Hat Creek basin. On the western margin of the basin just north of SL, Hat Creek flows near the basalt-flow aquifer—OV contact, resulting in a potential pathway for surface-water/groundwater exchange, with multiple basalt-flow aquifers, where lava flows are thinnest and closest to exposure at the surface (Fig. 6b). Another conceptual cross-section (Fig. 6a) depicts the flow of the creek along the western margin of the HCB near the contact with the Sugarloaf edifice aquifer. The

exact architecture of the edifice/basalt-flow contacts is unknown, but Fig. 6 conceptually demonstrates interfingering between the edifice and basalt-flow units. In addition to hydraulic connection at lava flow margins, incision by streams through thin parts of the basalts can provide connection with the aquifer system (Fig. 6a). High-volume springs discharge at both structural and depositional boundaries (Fig. 5); including from the upthrown side of faults (e.g., Lost Creek headwater spring), at potential fault barriers (e.g., Big Spring), or at the terminus of volcanic features (e.g., Rising River spring at the distal end of the HCB and margin of the Cinder Butte edifice).

Streamflow and stream temperature: locations of groundwater/surface-water interactions

Combining streamflow and temperature measurements allows the identification of an alternating pattern of stream gains from springs and losses from stream leakage along Hat Creek (Fig. 7). The late summer 2019 seepage-run measurement locations were selected after using the 2018 TIR survey data to identify gaining stream reaches. Synoptic seepage-run data from 2019 and previous years illustrate the general pattern of alternating gains and losses (dashed line on Fig. 7). TIR data allow identification of short reaches where most stream gains occur (gray bands on Fig. 7).

Prior seepage-run and streamflow measurements generally match the 2019 data, indicating that the pattern is robust, with modest variation over decades (Fig. 7). The range of late-season streamflow measured at the Hat Creek streamgage (Fig. 7) demonstrates that the 2019 pattern at that location is less than the median of the 78 years of data, but well within the decadal variation captured by the 10th and 90th percentiles. Near river km 14, low streamflow and narrow stream width precluded estimating temperature with the TIR imagery, resulting in the gap in median temperature data in Fig. 7. The resultant data gap extends downstream to the confluence with the spring-fed Rising River.

Fig. 6 Cross sections from the conceptual 3D diagram of the hydrogeology of the Hat Creek basin looking north. Cross-section locations are shown in Fig. 5. Each cross-section depicts a different interpretation of the relationship between the geology and the hydrogeology of the region. The red star, LS, identifies Lost Creek headwater spring, orange lines depict conceptual groundwater-flow directions. **a** Cross section, from a to a' in Fig. 5, depicts conceptual groundwater flow in the south of the study area, crossing Sugarloaf Peak. The potentiometric surface (dashed line with triangle) lies above the Hat Creek, driving groundwater flow into the creek. **b** Hat Creek lies above the aquifer and loses to it through the exposed contact. The aquifer behaves in an unconfined manner near the western margin of the valley and a confined manner to the east, by Lost Creek. Lost Creek neither gains nor loses to the groundwater system. **c** Hat Creek flows in the middle of the valley, and though the potentiometric surface for the uppermost aquifer lies below the creek, no pathway connects the creek to the aquifer; Hat Creek neither gains nor loses to the groundwater system. The relatively low potentiometric surface beneath Lost Creek drives water from the creek down the pathways provided by joints, cracks and fractures; here, Lost Creek loses to the groundwater system

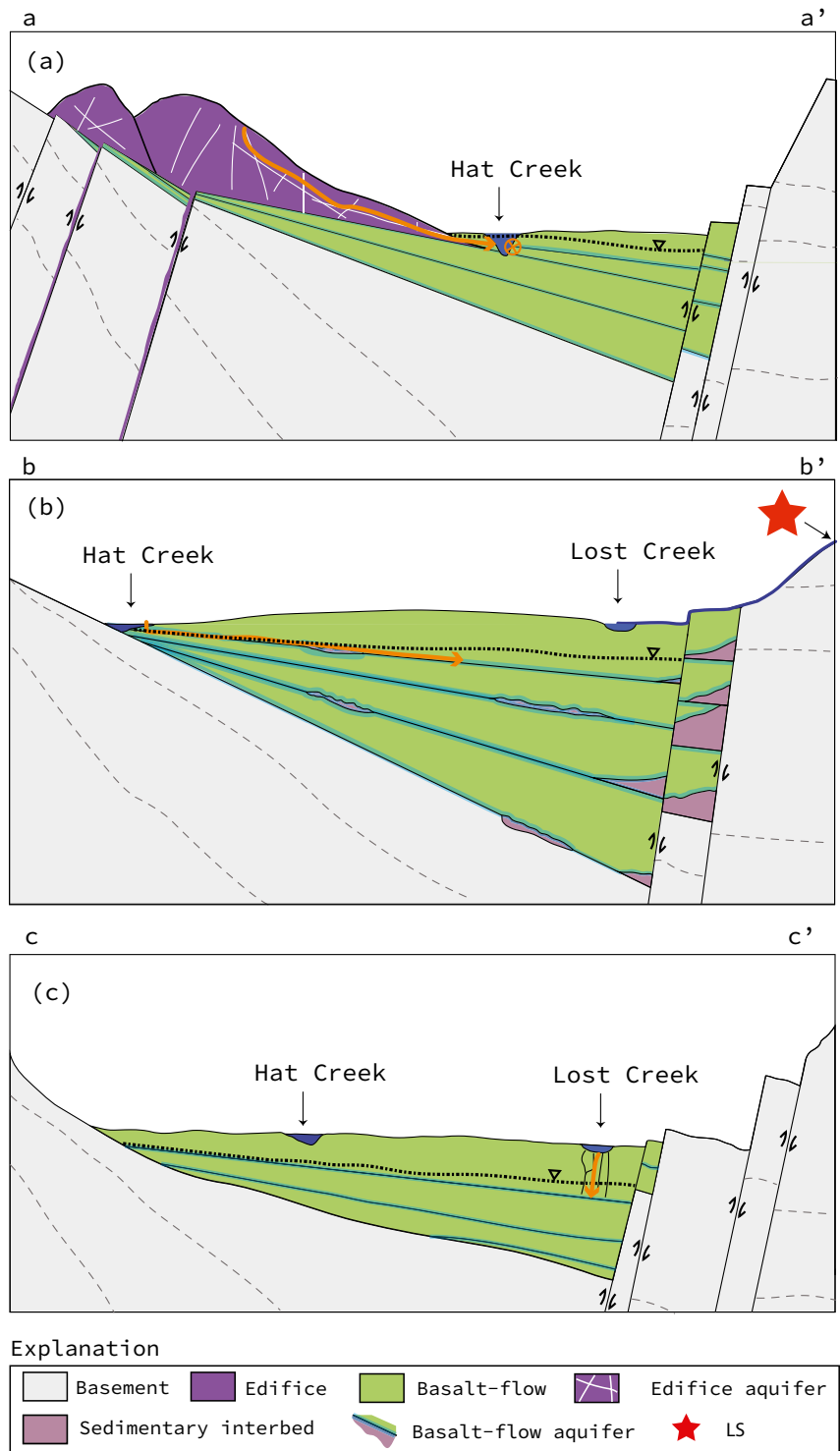
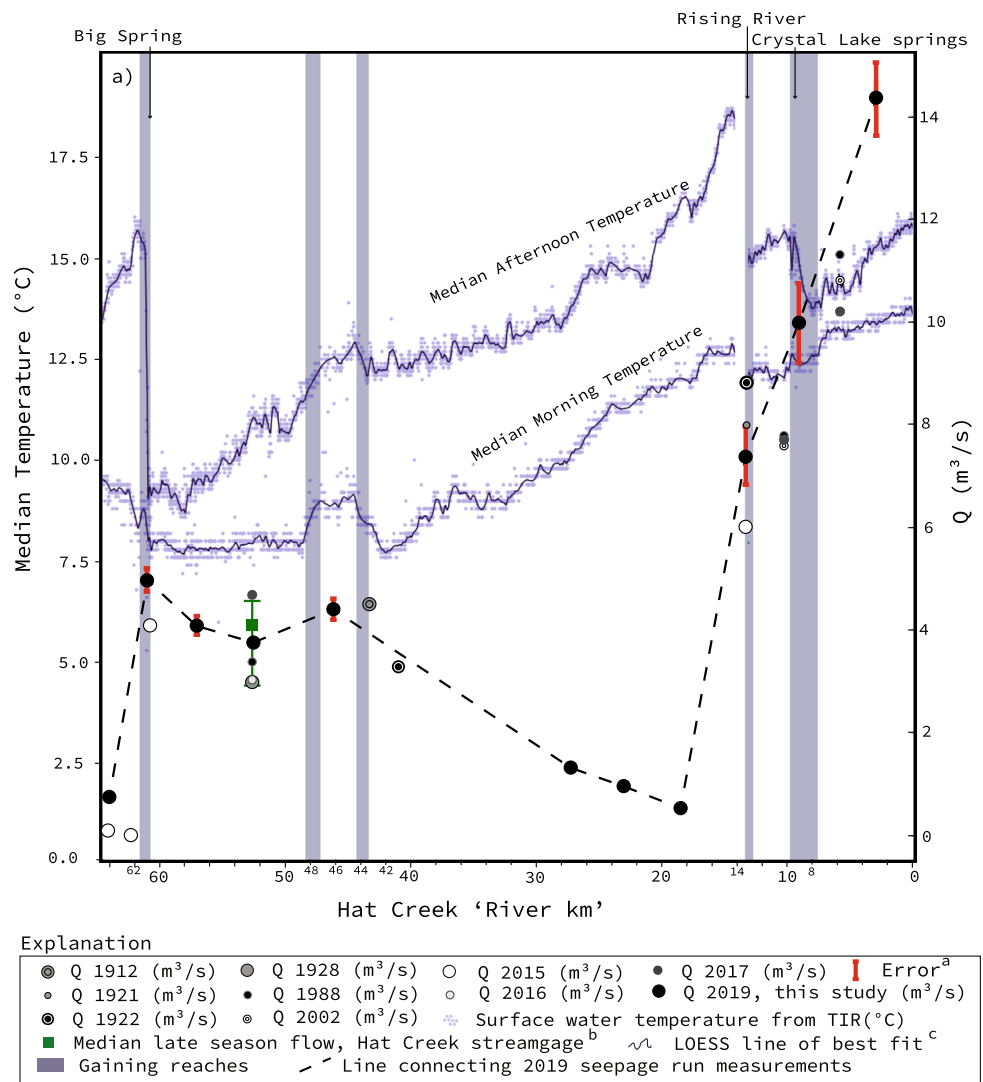


Fig. 7 Streamflow (Q , US Geological Survey 2019a) and September 24 and 25, 2018, afternoon and morning water-surface temperature along the length of Hat Creek. The $\sim 1 \text{ m}^3/\text{s}$ flow at river km 65 is Hat Creek flow from the watershed above, starting with low-volume springs near Lassen Peak (Fig. 2). Values from 2019 with no visible red whiskers have errors smaller than the width of the point representing them. Spring complexes are labeled. Streamflow is measured on the right axis and temperature on the left. Legend notes: ^aError categories: 5% (fair) or 8% (poor) of the measured value; ^bStreamgage for 1928–1930, 1960–1993, and 2016–2019 with whiskers denoting the 10th and 90th percentiles ^cCleveland (1979)



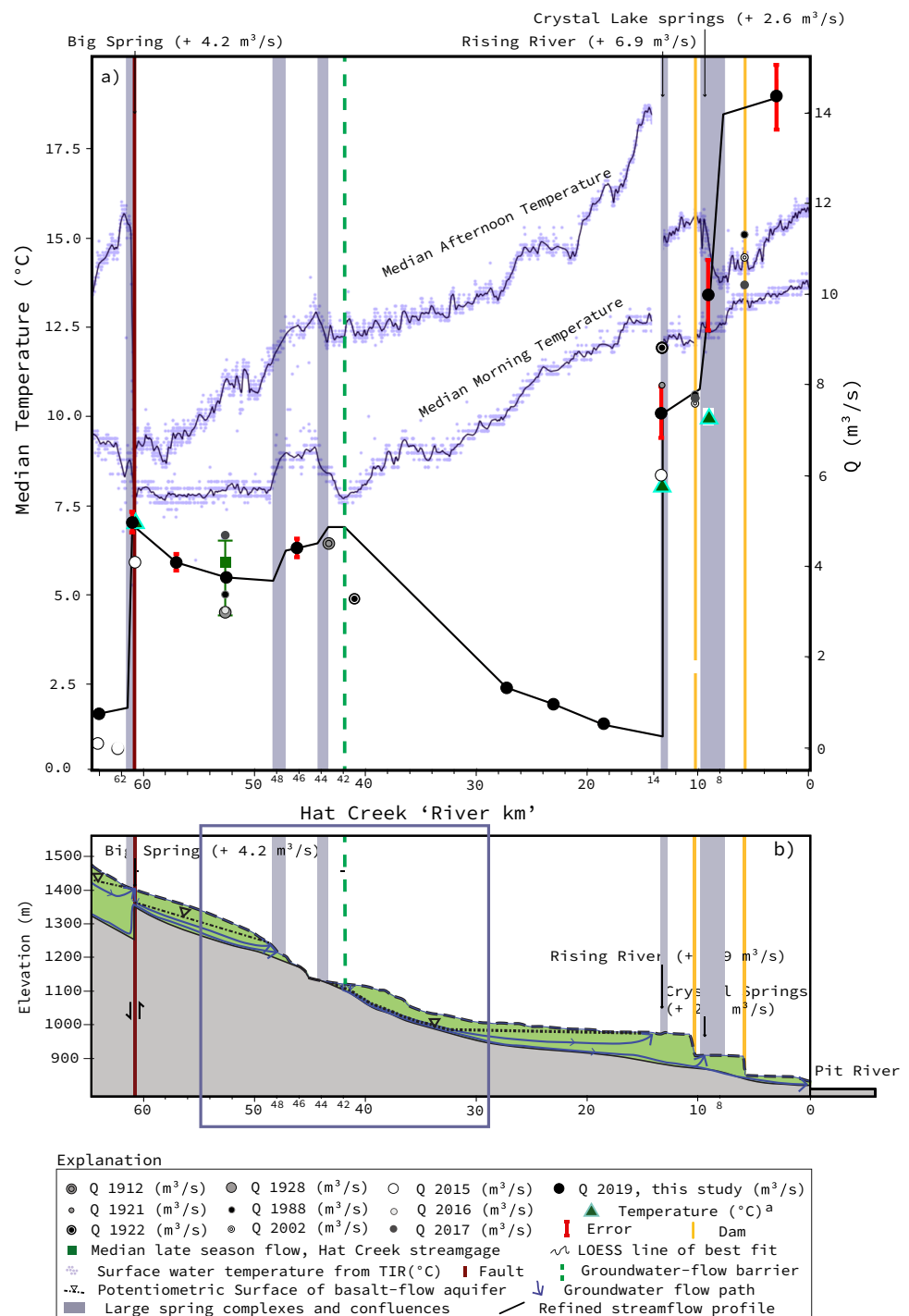
Discussion

Conceptual cross sections of geology and creek elevation (Fig. 8b), combined with streamflow and stream-temperature measurements (Fig. 8a), provide a refined understanding of the hydrogeology of the Hat Creek basin and spring-flow estimates at geologic features (Fig. 8a). Within the Hat Creek basin study area, the basin-filling basalt-flow aquifers are likely the dominant aquifers exchanging water with Hat Creek, but some spring sources may be from adjacent OV aquifers. As with the Hat Creek on the surface, the dominant groundwater flow direction is primarily from Lassen Peak in the south toward the Pit River in the north; but locally, groundwater is likely flowing through highly heterogenous flow paths from the adjacent horsts (part of unit OV) into the Hat Creek basin bottom aquifers.

Geologic evidence for groundwater-flow barriers

The changes in the permeability or continuity of an aquifer that impede groundwater flow and result in groundwater discharge are called groundwater-flow barriers. Faults and permeability juxtapositions between depositional units are two examples of groundwater-flow barriers; but under this general definition, depositional pinch-outs where basalts onlap high-elevation older less-permeable rocks can also form barriers to groundwater flow. Whereas springs do collocate with faults (Keegan-Treloar et al. 2022), exact mechanisms of fault controls on springs are poorly understood; though they can relate to fault offsets, bends, and volcanism potentially associated with feeder dikes within faults. The fault that coincides with Big Spring (Figs. 3 and 8b) is an example of a structural groundwater-flow barrier that likely juxtaposes the

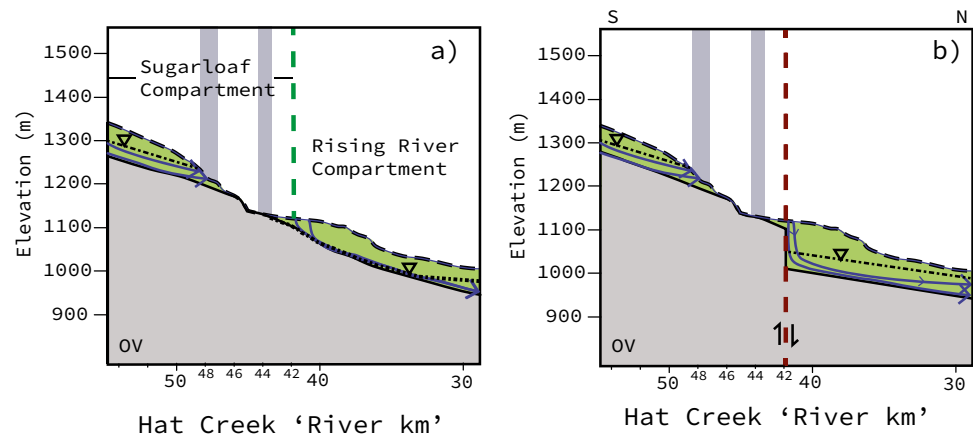
Fig. 8 Longitudinal profile of Hat Creek with respect to **a** the reinterpretation of Fig. 7 streamflow (solid line) based on TIR temperature estimates and streamflow and **b** elevation of the land surface. The seepage run and TIR survey data are from Fig. 7. **a** Discharge and temperature measurements along the longitudinal profile of Hat Creek are used to refine the streamflow profile (solid black line). **b** Hat Creek longitudinal profile depicts land-surface elevation, hydrogeologic units, and groundwater-flow paths. Two conceptual hydrogeologic units are present: the OV unit (older volcanics, gray) and the basalt-flow aquifer unit (green). Although the basalt-flow hydrogeologic unit is conceptualized as multiple thin aquifers at interflow zones separated by dense, impermeable lava-flow interiors, for simplicity, only one basalt-flow aquifer is depicted. The potentiometric surface of the uppermost aquifer is shown conceptually at land surface for gaining, and below for losing. Groundwater-flow barriers result in step changes in potentiometric surfaces, consistent with gaining and losing reaches. The elevations demarcated on the left apply only to the longitudinal elevation profile, not to the subsurface, which is vertically exaggerated to demonstrate surface-water/groundwater interactions. Potential groundwater-flow barriers are marked as either vertical red line (the fault at Big Spring) or dashed green. Legend note: ^aDavison and Rose (1997)



high and low permeability sections of lava flows. Controls on the groundwater-flow barrier on the north side of the Sugarloaf Peak (inset box in Fig. 8b), in the lowest reach of the Sugarloaf compartment, are less obvious. Two alternate models for the north-side springs are proposed (Fig. 9). In one explanation, the basalt-flow overlies the OV unit and the basalt-flow aquifer on the northeast of the volcano, disrupting the lateral continuity

of the basalt-flow aquifers, and allowing groundwater to leak from the aquifer margin (Fig. 9a). Alternatively (Fig. 9b), because the basalt-flow-aquifer may be continuous to the east (Fig. 3), a fault (as evidenced by the linear chain of cinder cones to the south and north of Sugarloaf Peak; Fig. 3) may still act as a barrier, making the collocation of the springs with OV part of the same story of fault offset.

Fig. 9 From the box in Fig. 8b. The two scenarios, **a** stratigraphic pinch-out and **b** structural offset, that explain groundwater/surface-water interaction north of Sugarloaf. See Fig. 8 explanation for details (OV older volcanics). The longitudinal profile of Hat Creek meanders along the floor of the basin from south to north, but as it approaches river km 42, it turns and flows from east to west (Fig. 3)



Compartmentalization of the aquifer system

In the Hat Creek basin, groundwater moves primarily from the south to the north, much as the Hat Creek does; however, the groundwater-flow paths in the Hat Creek are compartmentalized. The groundwater-flow barriers described in section ‘[Geologic evidence for groundwater-flow barriers](#)’ divide the focus area into leaky compartments. Within each compartment, stream gains and losses can be attributed to the existence of pathways to the groundwater system and the potential created by the relative relationship between potentiometric surface and stream stage. Figure 8b illustrates how barriers can create conditions for high potentiometric surfaces upstream of barriers (potential for springs), followed by low potentiometric surfaces downstream (potential for stream infiltration). Groundwater discharge zones define the downstream boundary of each compartment, whereas losing stream reaches define the upstream of the next compartment downstream. In the upper two compartments, this gain/loss pattern coincides to where Hat Creek runs across (W–E/E–W) known or inferred faults/general structural grain (N–S/NW–SE) of the Hat Creek basin (Fig. 3). Pathways for stream loss generally coincide where Hat Creek flows on the western margin of the basin and where lava flows are thinnest and closest to exposure at the surface (Figs. 6b and 8). Although fault damage zones are sometimes postulated to serve as vertical flow conduits (Caine et al. 1996), absence of a flow barrier would not result in low head downstream of the fault. Thus, steadily losing reaches downstream of the springs would not occur (i.e., a head drop from above land surface to below land surface at the fault is required to explain large springs above large stream loss reaches). Transitions from gaining to losing reaches at known or inferred groundwater barriers are used to subdivide the Hat Creek basin into three leaky hydrogeologic compartments (Fig. 8b). More compartments/barriers may exist within the valley bottom to the east of Hat Creek,

and compartment shape is poorly understood, but this manuscript focuses on the three identified compartments. Hereafter, the Big Spring compartment lies upstream of river km 61, the Sugarloaf compartment lies between river km 61 and 42, and the Rising River compartment occurs downstream of river km 42.

Big Spring compartment

The focus area and all associated plots consider only the first ~64 km of Hat Creek from the mouth, where TIR data are available, even though the headwaters of Hat Creek are ~78 km to the south of Pit River. Springs and the resulting Hat Creek flow are comparatively low in volume upstream of Big Spring (Fig. 8a; Rose et al. 1996). Hat Creek flow is $<1 \text{ m}^3/\text{s}$ at 64 km near where the TIR data begin. The Big Spring fault is a groundwater-flow barrier and forces $\sim 4.2 \text{ m}^3/\text{s}$ of groundwater into Hat Creek where Hat Creek travels NE across the NW–SE trending fault (Figs. 2 and 8a). Uniform and relatively low streamflow ($\sim 0.7 \text{ m}^3/\text{s}$) upstream of the Big Spring complex results in atmospheric heating and cooling and less buffering of diurnal temperature fluctuations (Fig. 8a), as lower volumes of water heat and cool faster than higher volumes (Caissie 2006). Between river km 62 and 61 upstream of the fault at Big Spring, streamflow increases by over 500%, resulting in cooling of both morning and afternoon stream temperatures over a ~1-km reach (Fig. 8).

Spring chemistry at Big Spring suggests multiple possible recharge areas (Rose et al. 1996), matching high-elevation sources including Table Mountain, Badger Mountain, Crater Peak part of Magee Volcano, and Lassen Peak (Fig. 1; Rose et al. 1996). Cell sizes for the recharge data (PRISM Climate Group 2015) are around 4 kilometers ($\sim 4 \text{ km}$), but tend to be 3.49 by 4.64 km in the SLMSA (PRISM Climate Group 2015). Multiplying the estimated average annual (from 1981–2010) precipitation of each pixel (green boxes, Fig. 2)

across the potential recharge area (259 km², Fig. 2) gives 11.3 m³/s of water. The 11.3 m³/s of water contributes to the evapotranspiration (ET) and recharge to aquifers that may feed Big Spring (PRISM Climate Group 2015; Fig. 2), and exceeds the measured 4.2 m³/s spring flow, leaving 7.1 m³/s for ET and groundwater flow past the spring. Recharge in the volcanic upper Deschutes River watershed is estimated to be up to 75% of precipitation (i.e., 25% ET), indicating that the proposed source of spring-flow at Big Spring (Rose et al. 1996) is viable. Average annual precipitation from Magee Volcano (yellow boxes, Fig. 2) adds an additional 2.7 m³/s of streamflow, meaning that Magee Volcano water is not strictly necessary to meet streamflow measured at Big Spring (though it may be a contributor). Thus, Magee Volcano cannot be the sole source of waters at Big Spring, due to the insufficient amount of water. The Big Spring compartment is likely leaky, and there might be alternate groundwater-flow paths from Lassen Peak around the compartment. This manuscript postulates that the average elevation of spring-water geochemistry measured likely reflects a range of elevations (Lassen Peak to Turner Mountain and its surroundings, Fig. 2) rather than one edifice (Crater Peak atop Magee Volcano, Fig. 2).

Sugarloaf compartment

The Sugarloaf compartment extends from the fault at Big Spring (ca. river km 61) to the groundwater-flow barrier north of Sugarloaf Peak (ca. river km 42; Fig. 8). The Sugarloaf compartment of Hat Creek loses streamflow over the upstream two-thirds and gains streamflow over the downstream third (Fig. 8a). Again, morning and afternoon stream temperatures change markedly over short reaches upstream of river km 48 suggesting localized groundwater discharge (Fig. 8). Between river kms 59 and 48, Hat Creek flows near or over a basalt-flow–edifice aquifer contact, this unit pinch-out could result in surface-water loss (Figs. 5 and 8). Modest temperature gains downstream between river kms 61 and 48 in the afternoon likely represent stream heating due to atmospheric exchange (Fig. 8a). Groundwater discharge could be from two different sources in the Sugarloaf compartment (Fig. 8), one warmer, potentially deeper flow path from Lassen Peak, heating both morning and afternoon stream temperatures near river km 48, and a second, colder source at river km 43 (Fig. 8a).

In the Sugarloaf compartment, streamflow losses upstream approximately balance downstream gains (Fig. 8). Possibly, stream losses upstream are regained downstream with little groundwater required from outside the compartment. Excess groundwater flow from nearby groundwater–recharge sources, including Crater Peak atop Magee Volcano, Table Mountain, and Badger Mountain (Rose et al. 1996; Fig. 2),

might leak through or past the downstream groundwater-flow barrier into the next compartment.

Rising River compartment

The Rising River compartment begins at the groundwater-flow barrier associated with Sugarloaf Peak (river km 42) and ends at the Pit River (river km 0). Groundwater mostly discharges near the northern terminus of Cinder Butte (Fig. 3; Tables 1 and 2) and the HCB, where topography drops as Hat Creek approaches the Pit River (Figs. 3 and 8b). The Rising River compartment loses streamflow in its upstream sections and gains in the downstream sections. North of Cassel, two sequential run-of-the-river dams divert water through turbines or allow the water to bypass. The local gage (US Geological Survey station 11358700) monitors only one diversion, so rarely if ever does the gage measure total streamflow (e.g., total water flowing past the dam through the diversion and bypass). From September 8–19, 2019, water diverted from Hat Creek for the upper dam's (southernmost dam, Fig. 3) operation was an average of 0.28 m³/s (US Geological Survey 2022). The low amounts of water diverted might indicate that most of this water is immediately used for the generation of electricity, flowing through turbines to Hat Creek below the powerhouse. The increase in Hat Creek streamflow at river kms 10 and 6 might be due to lower dam operations (northernmost dam, Fig. 3), but because run-of-the-river-dams are defined by low storage capacity, both dams are assumed to affect streamflow to a small degree when compared to the ~6 m³/s gains measured near river km 9 (Fig. 8). Instead, streamflow gains are likely driven by spring flow added to Hat Creek from deeper groundwater-flow paths that add water below the surface of the Hat Creek.

Hat Creek loses close to 4.5 m³/s of streamflow between the groundwater-flow barrier (river km 42) and the confluence with the spring-fed Rising River (river km 14). Much of the 4.5 m³/s of streamflow lost above river km 14 may return to Hat Creek via Rising River headwater springs, which adds at least 6.9 m³/s of streamflow at the toe of Cinder Butte (Fig. 8). Rising River springs could also have additional sources of groundwater from the uplands to the east.

In addition to the thermal effect of the lake associated with Crystal Lake springs, stream temperatures are potentially influenced by the dams (Fig. 8). Most of the streamflow (~14.3 m³/s) measured near river km 3 likely enters Hat Creek before river km 7, as evidenced by the TIR data (Fig. 8) and originates from the Crystal Lake springs complex as distributed seepage.

Isotopic compositions found in the Rising River compartment at Rising River and Crystal Lake springs indicate a Lassen

Peak source for at least some of the springs (Rose et al. 1996). These data suggest a deeper groundwater-flow path via leakage through or around the upstream compartments. This is unsurprising, as the geology suggests that all the basalt-flow aquifers pinch out as Hat Creek flows into the Pit River (Fig. 8b).

Implications for other volcanic terranes

Groundwater systems in volcanic regions with vertical displacement on faults could be compartmentalized. Comparing the proposed relationship between fault throw and compartmentalization to the well-studied upper Deschutes River and upper Klamath River basins (Gannett et al. 2001, 2007) might give more insight. Though previous work analyzes these basins at large scales, the relationship between groundwater-flow barriers and structure and stratigraphy is not as fully examined as the detailed work herein. In the upper Deschutes River drainage basin, Tertiary to Quaternary volcanic rocks interact with the Brothers, Sisters, and Green Ridge section of the Metolius fault zones (Gannett et al. 2001); whereas, the upper Klamath River basin hosts volcanic rocks that are faulted and as old as the pre-Tertiary and can locally be compartmentalized by faults (Gannett et al. 2007). Both drainage basins lie in regions where faulting and arc volcanism intersect (Blakely et al. 1997; Gannett et al. 2007; Waldien et al. 2019). Moreover, both basins contain rocks that are markedly older and have lower permeability, indicating possible permeability reduction with increased alteration to clay (Jefferson et al. 2010; Burns et al. 2015, 2017a), which would enable a more comprehensive study of the relationship between compartmentalization, faulting and age/alteration.

Summary and future work

An investigation based on detailed geologic maps, well logs, streamflow data, and TIR imagery collected in the morning and late afternoon result in a detailed conceptual model of the hydrogeology and groundwater/surface-water exchanges of the lower Hat Creek basin. These investigations reveal aspects of specific geologic features associated with both warm- and cold-water anomalies in Hat Creek's longitudinal stream temperature profile. In rivers without TIR imagery, additional research would be needed to assess whether LiDAR topographic data can be used to characterize the geology (e.g., faults and stratigraphic contacts) associated with longitudinal thermal heterogeneity and cold-water refuges important for cold-water species (Fullerton et al. 2018). Because of the lack of data, this paper does not attempt to pinpoint exact groundwater-flow paths, but rather attempts to constrain them through the Hat Creek basin. Measurements

of hydraulic head and conductivity (k) are available for only a small part of the Hat Creek basin, but would greatly increase understanding of the Hat Creek basin groundwater system.

Conclusions

Hat Creek flows over a leaky, compartmentalized aquifer system with at least three distinct segments separated by geologic structures. The two downstream compartments are characterized by losing stream reaches upstream and gaining reaches downstream. This manuscript hypothesizes that the pattern of streamflow gain followed by streamflow loss occurs across structural boundaries created by faults and at unconformities between volcanic units with contrasting transmissivity. The upstream-most Big Spring compartment gains $4.2 \text{ m}^3/\text{s}$ at its downstream boundary near the fault at Big Spring, increasing streamflow by a factor of 5. The Sugarloaf compartment likely regains streamflow lost in its upstream reaches at a groundwater-flow barrier between river kms 48 and 42. In the Rising River compartment, near river km 15, Hat Creek almost goes dry, but gains around $14 \text{ m}^3/\text{s}$ between river kms ~ 14 and 8. Similar patterns of streamflow gains and loss at groundwater-flow barriers can be found at other locations in the Shasta-Lassen Peak-Medicine Lake volcano study area (SLMSA) south of the Pit River, and likely in other regions with similar geologic features. Northern SLMSA shows a pattern of drainage and spring discharge controlled by the depositional extent of volcanic units. In the case of the Hat Creek basin, the use of the spatially extensive airborne thermal infrared (TIR) remote sensing dataset reveals the relationship between structure, stratigraphy, and groundwater/surface-water interactions. Extrapolating the methods used in this study to other regions characterized by coeval faulting and volcanism, such as the Klamath and Deschutes River drainage basins, might lead to a similar depth of understanding of their hydrogeologic systems.

Acknowledgements The authors contracted with Quantum Spatial, Inc. (now NV5 Geospatial) to acquire the airborne TIR imagery for this study; S. Venables and M. Diabat collected and processed the data, respectively. S. Wheelock and A. Slotke along with the US Forest Service, Lassen National Forest, Hat Creek Ranger District, provided field support in deploying and retrieving water temperature data loggers. Thanks also to D. Sweetkind, with the US Geological Survey, Geosciences and Environmental Change Science Center, for his help in the field. The authors would also like to thank M. Appold, G.E. Fogg, T.R. Jackson and one unnamed reviewer for their efforts in reviewing and editing this article. Any use of trade, product or firm names is for descriptive purposes only and does not imply endorsement by the US Government.

Funding Funding for this project was provided from the US Geological Survey Water Availability and Use Science Program. Additional funding for Erick Burns was provided by the US Dept. of Energy - Geothermal Technologies Program (EERE award number DE-EE0007169) and the US Geological Survey Energy Resources Program.

Declarations

Conflict of interest On behalf of all authors, the corresponding author states that there is no conflict of interest.

Open Access This article is licensed under a Creative Commons Attribution 4.0 International License, which permits use, sharing, adaptation, distribution and reproduction in any medium or format, as long as you give appropriate credit to the original author(s) and the source, provide a link to the Creative Commons licence, and indicate if changes were made. The images or other third party material in this article are included in the article's Creative Commons licence, unless indicated otherwise in a credit line to the material. If material is not included in the article's Creative Commons licence and your intended use is not permitted by statutory regulation or exceeds the permitted use, you will need to obtain permission directly from the copyright holder. To view a copy of this licence, visit <http://creativecommons.org/licenses/by/4.0/>.

References

- Anderson CA (1940) Hat Creek lava flow. *Am J Sci* 238(7):477–492. <https://doi.org/10.2475/ajs.238.7.477>
- Atwater T (1970) Implications of plate tectonics for the Cenozoic tectonic evolution of western North America. *Geol Soc Am Bull* 81(12):3513–3536. [https://doi.org/10.1130/0016-7606\(1970\)81\[3513:IOPTFT\]2.0.CO;2](https://doi.org/10.1130/0016-7606(1970)81[3513:IOPTFT]2.0.CO;2)
- Austin LJ (2013) Evolution of regional stress state based on faulting and folding near the Pit River, Shasta County, California. MSc Thesis, University of Oregon, Eugene, OR
- Blakely RJ, Christiansen RL, Guffanti M, Wells RE, Donnelly-Nolan JM, Muffler LJP, Clynne MA, Smith JG (1997) Gravity anomalies, Quaternary vents, and Quaternary faults in the southern Cascade Range, Oregon and California: implications for arc and backarc evolution. *J Geophys Res: Solid Earth* 102(B10):22513–22527. <https://doi.org/10.1029/97JB01516>
- Blakeslee MW, Kattenhorn SA (2013) Revised earthquake hazard of the Hat Creek fault, northern California: a case example of a normal fault dissecting variable-age basaltic lavas. *Geosphere* 9(5):1–13. <https://doi.org/10.1130/GES00910.1>
- Burns ER, Morgan DS, Peavler RS, Kahle SC (2011) Three-dimensional model of the geologic framework for the Columbia Plateau Regional Aquifer System, Idaho, Oregon, and Washington. *US Geol Surv Sci Invest Rep* 2010-5246. <https://doi.org/10.3133/sir20105246>
- Burns ER, Morgan DS, Lee KK, Haynes JV, Conlon TD (2012) Evaluation of long-term water-level declines in basalt aquifers near Mosier, Oregon. *US Geol Surv Sci Invest Rep* 2012-5002. <https://doi.org/10.3133/sir20125002>
- Burns ER, Williams CF, Ingebritsen SE, Voss CI, Spane FA, Deangelo J (2015) Understanding heat and groundwater flow through continental flood basalt provinces: insights gained from alternative models of permeability/depth relationships for the Columbia Plateau, USA. *Geofluids* 15(1–2):120–138. <https://doi.org/10.1111/gfl.12095>
- Burns ER, Williams CF, Tolan T, Kaven JO (2016) Are the Columbia River Basalts, Columbia Plateau, Oregon and Washington, USA, a viable geothermal target? A preliminary analysis. *Proc. 41, Forty-first Workshop on Geothermal Reservoir Engineering* Stanford University, Stanford, CA, February 22–24, 2016. <https://pubs.er.usgs.gov/publication/70169298>. Accessed Sept 2022
- Burns ER, Gannett MW, Sherrod DR, Keith MK, Curtis JA, Bartolino JR, Engot JA, Scandella BP, Stern MA, Flint AL (2017a) Geothermal implications of a refined composition-age geologic map for the volcanic terrains of southeast Oregon, northeast California, and southwest Idaho, USA. *GRC Trans* 41. <https://pubs.er.usgs.gov/publication/70191365>. Accessed Sept 2022
- Burns ER, Zho Y, Zhan H, Manga M, Williams CF, Ingebritsen SE, Dunham JB (2017b) Thermal effect of climate change on groundwater-fed ecosystems. *Water Resour Res* 53(4):3341–3351. <https://doi.org/10.1002/2016WR020007>
- Caine JS, Evans JP, Forster CB (1996) Fault zone architecture and permeability structure. *Geology* 24(11):1025–1028. [https://doi.org/10.1130/0091-7613\(1996\)024<1025:FZAAPS>2.3.CO;2](https://doi.org/10.1130/0091-7613(1996)024<1025:FZAAPS>2.3.CO;2)
- Caissie D (2006) The thermal regime of river: a review. *Freshw Biol* 51(8):1389–1406. <https://doi.org/10.1111/j.1365-2427.2006.01597.x>
- Casas-Mulet R, Pander J, Ryu D, Stewardson M, Geist J (2020) Unmanned aerial vehicle (UAV)-based thermal infra-red (TIR) and optical imagery reveals multi-spatial scale controls of cold-water areas over a groundwater-dominated riverscape. *Front Environ Sci* 8(64). <https://doi.org/10.3389/fenvs.2020.00064>
- Cleveland WS (1979) Robust locally weighted regression and smoothing scatterplots. *J Am Stat Assoc* 74(368):829–836. <https://doi.org/10.1080/01621459.1979.10481038>
- Clynne MA, Muffler LJP (2010) Geologic map of Lassen Volcanic National Park and vicinity, California. *US Geol Surv Sci Invest Map* 2899, scale 1:50,000. <https://pubs.usgs.gov/sim/2899/database.html>. Accessed 1 Sept 2018
- Clynne MA, Muffler LJP (2017) Geologic field-trip guide to the Lassen segment of the Cascades Arc, northern California. *US Geol Surv Sci Invest Rep* 2017-5022. <https://doi.org/10.3133/sir20175022K2>
- Colgan JP, Dumitru TA, Reiners PW, Wooden JL, Miller EL (2006) Cenozoic tectonic evolution of the Basin and Range Province in northwestern Nevada. *Am J Sci* 306(8):616–654. <https://doi.org/10.2475/08.2006.02>
- Curtis JA, Burns ER, Sando R (2020) Regional patterns in hydrologic response, a new three-component metric for hydrograph analysis and implications for ecohydrology, Northwest Volcanic Aquifer Study Area, USA. *J Hyrol Regional Studies* 30:100698. <https://doi.org/10.1016/j.ejrh.2020.100698>
- Curtis JA, Torgersen CE, Diabat M, Mejia FH, Marcelli MF, Burns ER, Wheelock SJ, Slotke A (2021) Airborne thermal infrared imagery and longitudinal stream temperature profiles, Hat Creek, California, August 2018. *US Geol Surv Data Release*. <https://doi.org/10.5066/P9DMJYT7>
- Davisson ML, Rose TP (1997) Comparative isotope hydrology study of groundwater sources and transport in the three cascade volcanoes of northern California. *Lawrence Livermore Natl. Lab*. <https://doi.org/10.2172/4074>
- Davisson M L, Rose TP (2014) Recharge and flow in the Medicine Lake Volcano-Fall Rivers Springs Groundwater Basin, California. *Environ Forensic* 15(1):66–77. <https://doi.org/10.1080/15275922.2013.873097>
- Downs DT, Clynne MA, Champion DE, Muffler LPJ (2020) Eruption age and duration of the ~9 km³ Burney Mountain dacite dome complex, northern California, USA. *Geol Soc Am Bull* 132(5–6):1150–1164. <https://doi.org/10.1130/B35240.1>
- Dugdale SJ, Bergeron NE, St-Hilaire A (2015) Spatial distribution of thermal refuges analysed in relation to riverscape hydromorphology using airborne thermal infrared imagery. *Remote Sens Environ* 160:43–55. <https://doi.org/10.1016/j.rse.2014.12.021>
- Fenneman NM, Johnson DW (1946) Physiographic divisions of the conterminous U.S. *US Geol Surv Map*, scale: 1:7,000,000. <https://water.usgs.gov/GIS/metadata/usgswrd/XML/physio.xml>. Accessed Sept 2022

- Fullerton AH, Torgersen CE, Lawler JJ, Faux RN, Steel EA, Beechie TJ, Ebersole JL, Leibowitz SG (2015) Rethinking the longitudinal stream temperature paradigm: region-wide comparison of thermal infrared imagery reveals unexpected complexity of river temperatures. *Hydrol Process* 29(22):4719–4737. <https://doi.org/10.1002/hyp.10506>
- Fullerton AH, Torgersen CE, Lawler JJ, Steel EA, Ebersole JL, Lee SY (2018) Longitudinal thermal heterogeneity in rivers and refugia for coldwater species: effects of scale and climate change. *Aquat Sci* 80(3):1–15. <https://doi.org/10.1007/s00027-017-0557-9>
- Gannett MW, Lite KE, Morgan DS, Collins CA (2001) Ground-water hydrology of the upper Deschutes Basin, Oregon. US Geol Survey Water Resour Invest Rep 00-4162. <https://doi.org/10.3133/wri20004162>
- Gannett MW, Lite KE Jr, La Marche JL, Fisher BJ, Polette DJ (2007) Ground-water hydrology of the upper Klamath Basin, Oregon and California. US Geol Surv Sci Invest Rep 2007-5050. <https://doi.org/10.3133/sir20075050>
- Gawthorpe RL, Leeder MR (2000) Tectono-sedimentary evolution of active extensional basins. *Basin Res* 12(3–4):195–218. <https://doi.org/10.1111/j.1365-2117.2000.00121.x>
- Gay TE, Aune QA (1958) Geologic map of California: Alturas sheet. California Div Mines Geol, scale 1(250):000. https://ngmdb.usgs.gov/ngm-bin/pdp/zui_viewer.pl?id=7641. Accessed Sept 2022
- Gingerich SB (1999) Ground-water occurrence and contribution to streamflow, northeast Maui, Hawaii. US Geol Surv Water Resour Invest Rep 99-4090
- Grossenbacher KA, McDuffie SM (1995) Conductive cooling of lava: columnar joint diameter and stria width as functions of cooling rate and thermal gradient. *J Volcanol Geotherm Res* 69:95–103. [https://doi.org/10.1016/0377-0273\(95\)00032-1](https://doi.org/10.1016/0377-0273(95)00032-1)
- Harris AJL (2013) Lava flows. In: Fagets SA, Gregg TKP, Lopes RMC (eds) Modeling volcanic processes: the physics and mathematics of volcanism. Cambridge University Press, London, pp 173–202
- Jefferson AJ, Grant G, Rose T (2006) The influence of volcanic history on groundwater patterns on the west slope of the Oregon High Cascades. *Water Resour Res* 42(12):1–15. <https://doi.org/10.1029/2005WR004812>
- Jefferson A, Grant G, Lewis SL, Lancaster ST (2010) Coevolution of hydrology and topography on a basalt landscape in the Oregon Cascade Range, USA. *Earth Surf Process Landf* 35(7):803–816. <https://doi.org/10.1002/esp.1976>
- Kattenhorn SA, Schaefer CJ (2008) Thermal–mechanical modeling of cooling history and fracture development in inflationary basalt lava flows. *J Volcanol Geotherm Res* 170(3–4):181–197. <https://doi.org/10.1016/j.jvolgeores.2007.10.002>
- Kattenhorn SA, Krantz B, Walker EL, Blakeslee MW (2016) Evolution of the Hat Creek fault system, northern California. In: Krantz B, Ormand C, Freeman B (eds) 3-D structural interpretation: earth, mind, and machine. *Am Assoc Petrol Geol Mem* 111, pp 121–154. <https://doi.org/10.1306/13561990M1113674>
- Keegan-Treloar R, Irvine DJ, Solórzano-Rivas SC, Werner AD, Banks EW, Currell MJ (2022) Fault-controlled springs: a review. *Earth Sci Rev* 230(1). <https://doi.org/10.1016/j.earscirev.2022.104058>
- Langenheim V, Jachens R, Muffler LJP, Clynne MA (2016) Implications for the structure of the Hat Creek fault and transfer of right-lateral shear from the Walker Lane north of Lassen Peak, northern California, from gravity and magnetic data. *Geosphere* 12(3):790–808. <https://doi.org/10.1130/GES01253.1>
- Le Corvec N, Spörl K, Bernhard J, Rowland J, Lindsay J (2013) Spatial distribution and alignment of volcanic centers: clues to the formation of monogenetic volcanic fields. *Earth Sci Rev* 24:96–114. <https://doi.org/10.1016/j.earscirev.2013.05.005>
- Lee J, Garwood J, Stockli DF, Gosse J (2009) Quaternary faulting in Queen Valley, California-Nevada: implications for kinematics of fault-slip transfer in the Eastern California Shear Zone–Walker Lane Belt. *Geol Soc Am Bull* 121(3–4):599–614. <https://doi.org/10.1130/B26352.1>
- Leeder MR, Gawthorpe RL (1987) Sedimentary models for extensional tilt-block/half graben basins. *Geol Soc Spec Publ* 28(1):139–152. <https://doi.org/10.1144/GSL.SP.1987.028.01.11>
- Lindholm GF (1996) Summary of the Snake River plain regional aquifer-system analysis in Idaho and eastern Oregon. US Geol Surv Prof Pap 1408-A. <https://doi.org/10.3133/pp1408A>
- Loheide SP, Gorelick SM (2006) Quantifying stream–aquifer interactions through the analysis of remotely sensed thermographic profiles and in situ temperature histories. *J Am Chem Soc* 40(10):3336–3341. <https://doi.org/10.1021/es0522074>
- Lyden PA, Gay TE, Jennings CW (1960) Geologic map of California: Westwood sheet. California Div Mines Geol Scale 1(250):000. https://ngmdb.usgs.gov/Prodesc/proddesc_371.htm. Accessed 1 June 2022
- Lyle P (2000) The eruption environment of multi-tiered columnar basalt flows. *J Geol Soc (London, UK)* 157(4):715–722. <https://doi.org/10.1144/jgs.157.4.715>
- Manga M (1997) A model for discharge in spring-dominated streams and implications for the transmissivity and recharge of Quaternary volcanics in the Oregon Cascades. *Water Resour Res* 33(8):1813–1822. <https://doi.org/10.1029/97WR01339>
- Manga M (2001) Using springs to study groundwater flow and active geologic processes. *Annu Rev Earth Planet Sci* 29(1):201–228. <https://doi.org/10.1146/annurev.earth.29.1.201>
- Manga M, Kirchner JW (2004) Interpreting the temperature of water at cold springs and the importance of gravitational potential energy. *Water Resour Res* 40(5). <https://doi.org/10.1029/2003WR002905>
- Marcelli MF, Peterson MF (2022) Data release of hydrogeologic data of the Hat Creek basin, Shasta County, California. US Geol Surv Sciencebase data release. US Geological Survey, Reston, VA
- McQuarrie N, Wernicke BP (2005) An animated tectonic reconstruction of southwestern North America since 36 Ma. *Geosphere* 1(3):147–172. <https://doi.org/10.1130/GES00016.1>
- Meinzer OE (1927) Large springs in the United States. US Geol Surv Water Suppl Pap 557
- Monk WA, Wilbur NM, Curry RA, Gagnon R, Faux RN (2013) Linking landscape variables to cold water refugia in rivers. *J Environ Manag* 118:170–176. <https://doi.org/10.1016/j.jenvman.2012.12.024>
- Muffler LJP, Clynne MA (2015) Geologic field-trip guide to Lassen Volcanic National Park and vicinity, California. US Geol Surv Sci Invest Rep 2015-5067. <https://doi.org/10.3133/sir20155067>
- Muffler LJP, Clynne MA, Champion DE (1994) Late Quaternary Normal Faulting of the Hat Creek Basalt, northern California. *Geol Soc Am Bull* 106(2):195–200. [https://doi.org/10.1130/0016-7606\(1994\)106<0195:LQNFOT>2.3.CO;2](https://doi.org/10.1130/0016-7606(1994)106<0195:LQNFOT>2.3.CO;2)
- Muffler LJP, Clynne MA, Calvert AT, Champion DE (2011) Diverse, discrete mantle-derived batches of basalt erupted along a short normal fault zone: the Poison Lake chain, southernmost Cascades. *Geol Soc Am Bull* 123(11–12):2177–2200. <https://doi.org/10.1130/B30370.1>
- O’Sullivan AM, Devito KJ, Curry RA (2019) The influence of landscape characteristics on the spatial variability of river temperatures. *Catena* 177:70–83. <https://doi.org/10.1016/j.catena.2019.02.006>
- O’Sullivan AM, Devito KJ, Ogilvie J, Linnansaari T, Pronk T, Allard S, Curry RA (2020) Effects of topographic resolution and geologic setting on spatial statistical river temperature models. *Water Resour Res* 56(12):1–23. <https://doi.org/10.1029/2020WR028122>
- Pollard DD, Aydin A (1988) Progress in understanding jointing over the past century. *Geol Soc Am Geol Soc Am Bull* 100(8):1181–1204. [https://doi.org/10.1130/0016-7606\(1988\)100<1181:PIUJO T>2.3.CO;2](https://doi.org/10.1130/0016-7606(1988)100<1181:PIUJO T>2.3.CO;2)

- PRISM Climate Group (2015) AN81 gridded climate dataset. Oregon State University. <http://prism.oregonstate.edu/>. Accessed 20 Jan 2020
- Rose TP, Davissou ML, Criss RE (1996) Isotope hydrology of voluminous cold springs in fractured rock from an active volcanic region, northeastern California. *J Hyrol* 179(1–4):207–236. [https://doi.org/10.1016/0022-1694\(95\)02832-3](https://doi.org/10.1016/0022-1694(95)02832-3)
- Thornton PE, Thornton MM, Mayer BW, Wei Y, Devarakonda R, Vose RS, Cook RB (2016) Daymet: daily surface weather data on a 1-km grid for North America, version 3. ORNL DAAC, Oak Ridge, TN. <https://doi.org/10.3334/ORNLDACC/1328>
- Torgersen CE, Faux RN, McIntosh BA, Poage NJ, Norton DJ (2001) Airborne thermal remote sensing for water temperature assessment in rivers and streams. *Remote Sens Environ* 76(3):386–398. [https://doi.org/10.1016/S0034-4257\(01\)00186-9](https://doi.org/10.1016/S0034-4257(01)00186-9)
- Turrin BD, Muffler LJP, Clynne MA, Champion DE (2007) Robust 24 ± 6 Ka $^{40}\text{Ar}/^{39}\text{Ar}$ age of a low-potassium Tholeiitic Basalt in the Lassen Region of NE California. *Quatern Res* 68(1):96–110. <https://doi.org/10.1016/j.yqres.2007.02.004>
- US Geological Survey (2019a) National Water Information System. US Geological Survey web interface. <https://doi.org/10.5066/F7P55KJN>. Accessed 17 Oct 2019
- US Geological Survey (2019b) US Geological Survey NED 1/3 arc-second n42w122 1 x 1 degree ArcGrid 2019, raster digital data. US Geological Survey, Reston, VA. <https://nationalmap.gov/elevation.html>. Accessed 23 March 2019
- US Geological Survey (2022) National Water Information System. US Geological Survey web interface. <https://doi.org/10.5066/F7P55KJN>. Accessed 5 May 2022
- US Geological Survey and California Geological Survey (2018) Quaternary fault and fold database for the United States. <https://www.usgs.gov/natural-hazards/earthquake-hazards/faults>. Accessed 12 Nov 2018
- Unruh J, Humphrey J (2017) Seismogenic deformation between the Sierran Microplate and Oregon Coast Block, California, USA. *Geology* 45(5):415–418. <https://doi.org/10.1130/G38696.1>
- Waldien TS, Meigs AJ, Madin IP (2019) Active dextral strike-slip faulting records termination of the Walker Lane belt at the southern Cascade arc in the Klamath graben, Oregon, USA. *Geosphere* 15(3):882–900. <https://doi.org/10.1130/GES02043.1>
- Wells RE, McCaffrey R (2013) Steady rotation of the Cascade . *Geology* 41:1027–1030. <https://doi.org/10.1130/G34514.1>
- Wesnousky SG (2005a) The San Andreas and Walker Lane Fault Systems, western North America: transpression, transtension, cumulative slip and the structural evolution of a major transform plate boundary. *J Struct Geol* 27(8):1505–1512. <https://doi.org/10.1016/j.jsg.2005.01.015>
- Wesnousky SG (2005b) Active faulting in the Walker Lane. *Tectonics* 24(3):TC3009. <https://doi.org/10.1029/2004TC001645>

Publisher's note Springer Nature remains neutral with regard to jurisdictional claims in published maps and institutional affiliations.